



JGR Biogeosciences

RESEARCH ARTICLE

10.1029/2020JG006044

Edward Schuur, Rosvel Bracho, and Gerardo Celis are co-equal authors.

Key Points:

- Fifteen years of measurements reveal tundra to be a persistent annual net source of carbon to the atmosphere where permafrost is degrading
- Plant and microbial activity increased from historical levels such that respiration losses in most years overwhelmed productivity gains
- The longer successional dynamics of plants suggests that respiration may outpace productivity for decades as an accelerating feedback to climate change

Supporting Information:

Supporting Information may be found in the online version of this article.

Correspondence to:

E. A. G. Schuur, ted.schuur@nau.edu

Citation:

Schuur, E. A. G., Bracho, R., Celis, G., Belshe, E. F., Ebert, C., Ledman, J., et al. (2021). Tundra underlain by thawing permafrost persistently emits carbon to the atmosphere over 15 years of measurements. *Journal of Geophysical Research: Biogeosciences*, 126, e2020JG006044. https://doi.org/10.1029/2020JG006044

Received 6 SEP 2020 Accepted 25 JAN 2021

Author Contributions:

Conceptualization: Edward A.G. Schuur

Formal analysis: Edward A.G. Schuur, Rosvel Bracho, Gerardo Celis Investigation: Edward A.G. Schuur, Rosvel Bracho, Gerardo Celis, E. Fay Belshe, Justin Ledman, Jason G. Vogel, Elizabeth E. Webb

Writing – original draft: Edward A.G. Schuur, Rosvel Bracho, Gerardo Celis Writing – review & editing: E. Fay Belshe, Chris Ebert, Justin Ledman, Marguerite Mauritz, Elaine F. Pegoraro,

© 2021. American Geophysical Union. All Rights Reserved.

Tundra Underlain By Thawing Permafrost Persistently Emits Carbon to the Atmosphere Over 15 Years of Measurements

Edward A.G. Schuur¹, Rosvel Bracho², Gerardo Celis¹, E. Fay Belshe³, Chris Ebert¹, Justin Ledman¹, Marguerite Mauritz^{1,4}, Elaine F. Pegoraro¹, César Plaza^{1,5,6}, Heidi Rodenhizer¹, Vladimir Romanovsky⁷, Christina Schädel¹, David Schirokauer³, Meghan Taylor^{1,9}, Jason G. Vogel², and Elizabeth E. Webb³

¹Center for Ecosystem Science and Society, Department of Biological Sciences, Northern Arizona University, Flagstaff, AZ, USA, ²School of Forest, Fisheries, and Geomatics Sciences, University of Florida, Gainesville, FL, USA, ³School of Natural Resources and Environment, University of Florida, Gainesville, FL, USA, ⁴University of Texas, El Paso, TX, USA, ⁵Departamento de Biología y Geología, Física y Química Inorgánica, Escuela Superior de Ciencias Experimentales y Tecnología, Universidad Rey Juan Carlos, Móstoles, Spain, ⁶Instituto de Ciencias Agrarias, Consejo Superior de Investigaciones Científicas, Madrid, Spain, ⁷University of Alaska, Fairbanks, AK, USA, ⁸Denali National Park and Preserve, Denali Park, AK, USA, ⁹Yale School of the Environment, Yale University, New Haven, CT, USA

Abstract Warming of the Arctic can stimulate microbial decomposition and release of permafrost soil carbon (C) as greenhouse gases, and thus has the potential to influence climate change. At the same time, plant growth can be stimulated and offset C release. This study presents a 15-year time series comprising chamber and eddy covariance measurements of net ecosystem C exchange in a tundra ecosystem in Alaska where permafrost has been degrading due to regional warming. The site was a carbon dioxide source to the atmosphere with a cumulative total loss of 781.6 g C m⁻² over the study period. Both gross primary productivity (GPP) and ecosystem respiration ($R_{\rm eco}$) were already likely higher than historical levels such that increases in $R_{\rm eco}$ losses overwhelmed GPP gains in most years. This shift to a net C source to the atmosphere likely started in the early 1990s when permafrost was observed to warm and thaw at the site. Shifts in the plant community occur more slowly and are likely to constrain future GPP increases as compared to more rapid shifts in the microbial community that contribute to increased $R_{\rm eco}$. Observed rates suggest that cumulative net soil C loss of 4.18–10.00 kg C m⁻²—8%–20% of the current active layer soil C pool—could occur from 2020 to the end of the century. This amount of permafrost C loss to the atmosphere represents a significant accelerating feedback to climate change if it were to occur at a similar magnitude across the permafrost region.

Plain Language Summary The Arctic is warming at twice the global average. Shifting environmental conditions including the degradation of permafrost affect the storage of carbon in plants and soils of tundra ecosystems. Carbon uptake by plant growth and carbon release by microbial respiration of soil organic matter both appear to have increased prior to and over 15 years of measurements in a tundra ecosystem in Alaska where permafrost has been degrading. But, carbon release to the atmosphere overwhelmed uptake on average, which leads to net release of carbon to the atmosphere and accelerates climate change.

1. Introduction

Global mean surface temperature has increased by about 1.0°C above pre-industrial levels primarily driven by carbon (C) emissions into the atmosphere as a result of human activity (IPCC, 2018). Observed temperature increases in the Arctic are 2–3 times this global average due to Arctic amplification (Pithan & Mauritsen, 2014; Winton, 2006), and projected temperatures for the region are expected to increase by 8°C by 2100 relative to a 1986–2005 baseline if global society continues to follow a high C emission scenario (IPCC, 2013; Riahi et al., 2011). Tundra and boreal ecosystem structure and function in high-latitude regions will be dramatically altered by these changes, in part as a result of direct and indirect effects of degrading permafrost (perennially-frozen ground; Meredith et al., 2019; Schuur & Mack, 2018). The permafrost region occupies 22%–24% of the exposed land surface in the Northern Hemisphere (Brown et al., 1998; Gruber, 2012; Obu

SCHUUR ET AL. 1 of 23



César Plaza, Heidi Rodenhizer, Vladimir Romanovsky, Christina Schädel, David Schirokauer, Meghan Taylor, Jason G. Vogel, Elizabeth E. Webb et al., 2019; Zhang et al., 2000), and record high temperatures in the permafrost have been documented at many long-term monitoring sites (Biskaborn et al., 2019). A recent Permafrost Carbon Network Model Intercomparison Project (MIP) projected a 90% loss of near-surface permafrost area by 2300 under a high C emission scenario, with much of that long-term loss already occurring by 2100 (McGuire et al., 2018).

One of the key consequences of changing permafrost ecosystems is the potential to influence the future rate of climate change. Permafrost region soils contain a large, climate-sensitive C pool that can be transferred to the atmosphere as the greenhouse gases carbon dioxide (CO_2) and methane (CH_4 ; Euskirchen et al., 2006; Schuur et al., 2008, 2013, 2015; Zhuang et al., 2006; Zimov et al., 2006). Total soil organic C in the northern circumpolar permafrost region is estimated to be 1,440–1,600 Pg C, stored in surface as well as deeper (>3 m) soil layers (Hugelius et al., 2014; Schuur et al., 2015, 2018; Strauss et al., 2017). This permafrost C pool is large compared to the 2,000 Pg organic soil C contained in the top 3 m of all other biomes around the world (Jobbágy & Jackson, 2000) and is concentrated in only 15% of the world's soil area (Schuur et al., 2015). The permafrost feedback to climate in a warmer world ultimately depends on how much of this C is released to the atmosphere, the timing of its release, and the proportion of C that is released as CH_4 or CO_2 (Schuur et al., 2013).

Warmer temperatures thaw permafrost (Romanovsky et al., 2012, 2017) and enhance microbial decomposition of stored organic soil C (Schädel et al., 2014, 2016). At the same time, plant growth can increase C storage in new plant biomass or deposit new soil organic matter. It is the net difference of these opposing C exchanges and their dynamics through time that determines the ultimate effect on atmospheric C (Koven et al., 2015; Schuur et al., 2008; Shaver et al., 2000). While the soil C pool for the circumpolar permafrost region is roughly 15 times larger than C stored in plant biomass (Schuur et al., 2018), the Permafrost Carbon MIP suggested that increased plant C uptake (greening) may occur quickly, stimulated both by warming conditions and CO2 fertilization. Greening was modeled to offset both current soil C losses (McGuire et al., 2016) as well as future losses over many decades through the end of this century (McGuire et al., 2018). It was only over the very long term (multiple centuries) when these models projected that continued soil C losses would overwhelm plant C uptake and lead to a significant accelerating feedback to climate warming. These model results, however, do not always match regional observations of significant vegetation decreases (browning) over some tundra (Bhatt et al., 2017; Bjerke et al., 2017; Lara et al., 2018; Phoenix & Bjerke, 2016) and boreal (Beck et al., 2011; Ju & Masek, 2016) regions. Nor do they correspond with a regional atmospheric snapshot that recorded the tundra and boreal regions of Alaska together as current net C sources to the atmosphere (Commane et al., 2017), or a synthesis of winter time ecosystem respiration loss that also suggested the permafrost region is currently an annual net C source (Natali et al., 2019).

The response of plants and soil in permafrost ecosystems to warming is likely to be a long-term dynamic with non-linear responses that change over annual to decadal time scales. The soil microbial community has the potential to respond quickly to environmental changes in moisture and temperature due to the fast reproduction rate and short life span of microbes. But, long-term C losses may originate largely from slowly-decomposing organic matter that comprises the majority of permafrost C emerging as a result of thaw (Bracho et al., 2016; Mueller et al., 2015; Schädel et al., 2014; Schuur & Abbott, 2011; Schuur et al., 2013). The plant community also has the potential to respond quickly to changing resource availability such as increased CO₂, nutrients, and temperature/growing season (Chapin et al., 1995; McGuire et al., 2012; Shaver et al., 2006). At the same time, changing environmental conditions may not always favor increased productivity of the existing plant community. For example, soil drying as a result of permafrost degradation may impact non-vascular plant species that represent a significant fraction of the plant community biomass and productivity (Deane-Coe et al., 2015; Osterkamp et al., 2009). Alternately, soil waterlogging as a result of ground ice melting and surface subsidence may inhibit plant growth (Natali et al., 2015). While an overall increase in resources should ultimately favor increased plant biomass and growth (Shaver et al., 2000), the shift in the environmental envelope beyond what has been historically experienced in these ecosystems (Koven et al., 2013) may lead to years-to-decades bottlenecks in dispersal and establishment of new plants that can benefit (Johnstone, Chapin, et al., 2010). This interplay between time scales and the balance between plant C uptake and microbial respiration of soil C ultimately controls the dynamics of C fluxes over the decades-to-century timescale relevant to the permafrost C feedback to climate.

SCHUUR ET AL. 2 of 23



This study addresses long-term C exchange dynamics in a tundra ecosystem in Interior Alaska underlain by permafrost that is degrading. Deep permafrost temperatures recorded since 1985 in a borehole at the site showed that changes in regional climate in the 1990s (Brown & Romanovsky, 2008) initiated permafrost degradation and ground subsidence through the early 2000s (Osterkamp et al., 2009; Schuur et al., 2009). Carbon cycle studies were started in 2004 initially using chamber net ecosystem C exchange (NEE) measurements (Belshe et al., 2012; Schuur et al., 2009; Trucco et al., 2012; Vogel et al., 2009), and were expanded in 2008 to a eddy covariance system (Belshe et al., 2012; Celis et al., 2017; Taylor et al., 2018) with a footprint that encompassed the patchwork of permafrost thaw measured by the chambers. This study site is unique because it is one of only a handful of sites in Alaska making continuous winter CO₂ flux measurements (Euskirchen et al., 2017; Oechel et al., 2014), and now has a long-term record that can be used to understand annual to decadal transition points in plant and soil processes where permafrost is actively degrading.

This time series was used to address key issues relating to ecosystem C balance in response to permafrost thaw, including: (1) what is the long-term (>decade) pattern and magnitude of NEE between tundra and the atmosphere?; (2) which environmental and ecosystem drivers control seasonal and interannual differences in GPP (gross primary productivity) and $R_{\rm eco}$ (ecosystem respiration) that together control NEE?; (3) what is the long-term contribution of non-summer season C emissions to total annual C exchange? (4) What is the likely fate of C dynamics in this ecosystem as the climate continues to warm? The time period covered by this study contains a wide range of climate variation including conditions that are demonstrably outside of the historical climate envelope of this tundra site. As such, it allows for a detailed examination of factors controlling uptake and release of C in a tundra ecosystem where permafrost is actively degrading, as a large fraction of the permafrost region is expected to undergo in the upcoming decades.

2. Materials and Methods

2.1. Study Site

The study site is characterized by moist acidic tundra within the Eight Mile Lake watershed (63°52′42.1″N, 149°15′12′W; 670 m above sea level), west of Healy, Alaska, USA (Schuur et al., 2007, 2009). Vascular plant cover is dominated by the tussock-forming sedge Eriophorum vaginatum and the deciduous shrubs Betula nana, Vaccinium uliginosum, and Rubus chamaemorus. Non-vascular biomass is dominated by mosses and lichens (Belshe et al. 2012; Deane-Coe et al., 2015; Natali et al., 2012). Soils are classified as Gelisols (Soil Survey Staff, 2014), with a thick organic horizon on top of cryoturbated mineral soil, which can accumulate up to 69 kg C m⁻³ (Pries et al., 2012). The long-term permafrost temperature record on site indicates warming of the permafrost, which led to ground subsidence (Osterkamp & Romanovsky, 1999; Osterkamp et al., 2009), and hydrologic redistribution creating a landscape with different levels of disturbance (Schuur et al., 2007, 2009; Vogel et al., 2009). The Eight Mile Lake research site is located within the larger Alaska Climate Division 3 region (AKCD3) as defined by the National Oceanic and Atmospheric Administration (NOAA; Bieniek et al., 2012). Long-term 30-year (1971–2000) mean annual air temperature (T_A) for the AKCD3 was -3.7° C \pm 1.2°C. Growing season (defined by the calendar, May 1 to September 30; most productive period of the year) $T_{\rm A}$ was 10.2°C \pm 3.8°C, and non-growing season (November 1 to March 31 of the following calendar year) T_A was -16.6°C ± 2.5 °C; monthly averages ranged from the warmest +14.0°C ± 1.0°C for July to the coldest -19.8°C ± 5.3°C for January. Average long-term annual precipitation was 378 mm, with a May to September mean of 245 mm (National Climatic Data Center, National Oceanic and Atmospheric Administration).

2.2. Ecosystem Carbon Dioxide Fluxes

NEE is largely the balance between two major opposing processes, the CO_2 uptake by primary producers (gross primary production GPP), and CO_2 losses by ecosystem respiration (R_{ecc} ; comprising autotrophic plant respiration and heterotrophic respiration; Chapin et al., 2006). NEE was measured using both chambers and eddy covariance (EC; Aubinet et al., 2000; Baldocchi, 2003) approaches over the full time series presented here, and these techniques overlapped at the site for one year (2008). Static and automated chamber systems were used in the site during the growing seasons from 2004 to 2008 (Schuur et al., 2009; Trucco et al., 2012; Vogel et al., 2009). Eighteen square plastic bases were placed during the summer of

SCHUUR ET AL. 3 of 23



2003 at locations spanning a gradient in permafrost degradation. Carbon exchange measurements for each season started after the snowmelt each year by placing 40 cm tall clear chambers on top of the bases. Air was circulated between the chambers and an infrared gas analyzer (IRGA, LI-820, Licor, Lincoln, and NE) at 1 L min⁻¹ for 1.5 min. Changes in CO₂ concentration were recorded every two seconds and CO₂ fluxes estimated from the change in CO₂ concentrations with time in the headspace of the chambers. Ecosystem respiration alone was measured during the nighttime in the auto chambers or by covering the static chambers with a dark shroud (for more details see Vogel et al., 2009). The EC system was established on an area that was representative of the chambers; measurements spanned from June 2008 until April 2019. The EC system comprised a sonic anemometer (CSAT3, Campbell Scientific Inc.) and an open path infrared CO₂/ H₂O analyzer (Li-7500 until May 2011 mounted on a 2 m tower and Li-7500A after June 2011 at 3.5 m, Licor Biosciences.). High frequency data were recorded at 10 Hz on a CR5000 datalogger (Campbell, Scientific, Logan Utah) until June 2015, and using a Li-COR interface unit (Li-7550, Licor Biosciences) until the end of the study. The CO₂/H₂O analyzer was calibrated at least twice a year using a zero CO₂ air source and a ±1% standard CO2 concentration close to atmospheric concentrations. Quality control on high frequency data was applied according to Foken et al. (2004). CO2 fluxes were estimated from the half-hourly averaged covariance of CO2 and vertical wind speed and then corrected for damping of high frequency fluctuations, sensors separation and misalignment of wind sensors with the local streamline, humidity correction of sonic temperature, (Foken et al., 2012; Schotanus et al., 1983), and density corrections (Webb et al., 1980). Fluctuations caused by surface heat exchange from the open path sensor (Li-7500) during wintertime conditions were also corrected (Burba et al., 2008); temperature in the IRGA sensor head (Li-7500A) was seasonally adjusted (Burba et al., 2008). We discarded 30-min fluxes from ±20° true south to avoid any influence of tower structure shadow on winds (Friebel et al., 2009). Our flux processing methodology was validated by Ameriflux Qa/Qc team visits to the site in 2012 and again in 2018, and by comparisons with flux calculations made using the open path Ameriflux gold standard files. A standard data screening protocol was applied to eliminate fluxes with systematic errors such as incomplete half-hour data sets, poor canopy coupling with the external atmospheric conditions as indicated by the friction velocity (u* threshold 0.12 m s⁻¹), footprint development (Kormann & Meixner, 2001), non-steady state conditions (Foken et al., 2004), and excessive spikes and rainy periods during the growing season. The amount of 30-min data remaining after the screening protocol ranged between 16% to 35% annually, 28% to 53% in the growing season, and 2% to 19% in the non-growing season, but was generally evenly distributed across months and seasons (Figure S1). We used the meteorological convention negative NEE represents C uptake by the ecosystem. Footprint climatologies were estimated under neutral stability conditions (Monin Ohbukov stability parameter (z-d)/ $L \ge -0.0625$ and $(z-d)/L \le 0.625$), and the area contributing to 80% of the measured fluxes corresponded to ~ 160 m diameter from the EC tower in the growing season (May to September) and about 230 m in the non-growing season (October to April; Taylor et al., 2018). Fetch extends about 300 m to the north side of the EC tower, and over 600 m in all other directions.

2.3. Ancillary Measurements

Standard meteorological data collected at \sim 2.5 m height from the beginning of the study included photosynthetically active radiation (PAR, Li-190SA, Li-COR Biosciences; PQS1, Kipp & Zonen), with PAR also measured inside the chambers to correct for reduced light transmission due to the chamber plastic material and structure; net radiation (R_n , REBS Q*7.1 net radiometer, REBS, and CNR4 Net radiometer, Kipp& Zonen); relative humidity (RH); and air temperature (T_A ; Vaisala HMP45C). A replicate set of sensors measured PAR, net radiation, T_A , and RH at a second meteorological tower 100 m NW of the EC tower and was used to gap fill using linear regressions. Soil temperature (T_S) was measured at 10 cm depth (T type thermocouples, Omega Eng.), and soil moisture integrated over the top 15 cm of soil (Stevens Hydra probe II, Stevens Water Monitoring Systems & CS615 and CS616, Campbell Scientific) at nine sites within the tower footprint, and at two sites located directly beneath the EC tower. Snow depth measurements started in the fall of 2012 (SR50A Sonic Ranging sensor, Campbell Scientific Inc.), with monthly averages ranging from 20 to 65 cm depth. Readings from all sensors were taken at least every minute and averaged over 30-min intervals by dataloggers (CR10X, CR1000, and CR5000 Campbell Scientific Inc., Sutron 9210-XLite, Sutron Corporation). Rainfall was measured using a HOBO Onset station during the growing season (Bourne, MA, USA). Thaw depth was measured biweekly throughout the growing season in at least nine different

SCHUUR ET AL. 4 of 23



locations representing the landscape within the EC tower footprint. Active layer thickness (ALT), the maximum extent of soil thaw at the end of the growing season, was reported as the average of the last two thaw depth (TD) measurement dates in September. Distance to the water table (water table depth, WTD) was measured manually with a ruler each week as the distance from moss/soil surface to the water table surface inside nine, 3-inch diameter PVC wells. WTD is reported on a negative scale since it was below the soil/ moss surface; smaller numbers (less negative) indicate wetter conditions with the water table closer the soil surface and more of the soil profile submerged. The enhanced vegetation index (EVI) measured at 250 m resolution at 16 days intervals (Didan et al., 2015), and daily snow cover measured at 500 m resolution (Hall & Riggs, 2016), both from MODIS, were used together to characterize greenness and phenology for the study area. The EVI and snow cover products were retrieved using the online Application for Extracting and Exploring Analysis Ready Samples (AppEEARS), courtesy of the NASA EOSDIS Land Processes Distributed Active Archive Center (LP DAAC), USGS/Earth Resources Observation and Science (EROS) Center, Sioux Falls, South Dakota, https://lpdaacsvc.cr.usgs.gov/appeears/. EVI data were processed using the Savitzky-Golay filter method that identifies abrupt changes not consistent with the gradual change in EVI (Chen et al., 2004); values that deviate more than 0.07 from the Savitzky-Golay estimate are filtered and interpolated from adjacent values. Air temperature measurements (T_A) were aggregated bi-weekly and seasonally as growing degree days (GDD, units $^{\circ}$ C) by summing all daily $T_{\rm A}$ averages $>0^{\circ}$ C within a given time period.

2.4. Flux Partitioning

Daytime conditions were assumed when PAR was >10 μ mol·m⁻²·s⁻¹; missing NEE values were filled using monthly (chambers) and biweekly (EC) parameters obtained by fitting measured NEE to PAR using a non-rectangular hyperbola (Falge et al., 2001) (nls, R, and R Core Team, 2018):

$$NEE_{day} = \frac{\infty \cdot PAR}{1 - (PAR / PAR_{max}) + (\infty \cdot PAR / GEE_{opt})} + R_d$$
 (1)

where α is the ecosystem quantum yield (µmol $CO_2 \cdot m^{-2} \cdot s^{-1}$ /µmol quantum· $m^{-2} \cdot s^{-1}$), GEE_{opt} (µmol $CO_2 \cdot m^{-2} \cdot s^{-1}$) is the optimum rate of CO_2 exchange at maximum observed PAR (PAR_{max}), and R_d is the ecosystem dark respiration (e.g., NEE at PAR = 0). The beginning and end of the growing season (detectable GPP) was determined when model and parameters estimated from fitting NEE measurements to PAR were significant (p < 0.05)

Within the April and October transition months when Equation 1 model and parameters were not statistically significant, and during the non-growing season, respiration conditions were dominant and a respiration gap filling strategy was applied. Ecosystem respiration ($R_{\rm eco}$) was gap filled by fitting nighttime growing season and winter NEE to air temperature at different times during day and year. If PAR during the growing season was <10 μ mol·m⁻²·s⁻¹, nighttime conditions were assumed and, if the fitting of NEE to PAR (Equation 1) was not significant in April, October and the non-growing season, winter conditions were assumed. $R_{\rm eco}$ was fitted to $T_{\rm A}$ using an exponential relationship (nls, R Core Team, 2018):

$$R_{\rm eco} = A \cdot e^{bT_A} \tag{2}$$

where A and b are parameters and T_A (°C) is half-hourly aggregated air temperature. Parameters were obtained using maximum likelihood. Half-hourly GPP was calculated as the difference between NEE and $R_{\rm eco}$. Monthly, seasonal and annual C balance, was obtained by aggregating measured and gap filled NEE.

2.5. Statistical Analysis

Analyses were based on phenological years, growing seasons, and non-growing seasons. The growing season is defined here based on site conditions as the period from May 1 to September 30, when the bulk of plant activity occurred. The non-growing season is the period from November 1 to March 31 when biological activity, especially at the ecosystem surface, is minimal. However, there are soil layers in the middle of the active layer profile that can remain unfrozen during at least part of that time. April is the transition

SCHUUR ET AL. 5 of 23



month from the non-growing season into the growing season and October is the transition month back into the non-growing season. In both of these months, there were weeks with statistically significant NEE/PAR relationships (Equation 1) indicating that plant C uptake had begun, but these were individual weeks at the end of April or beginning of October and not the full months. The phenological year (as opposed to the calendar year) was the period from May 1 to April 30 of the following year, with the named year (201x) corresponding with the summer growing season of that calendar year.

Cumulative annual C fluxes were related to mean annual environmental variables (mean annual T_A , T_S) in order to determine what drivers were the most significant explaining interannual variability in C dynamics. On a seasonal basis, we performed a principal component (PC) analysis on environmental and biological drivers (GDD, PAR, WTD, vapor pressure deficit (VPD), TD, TS, Precipitation, and EVI) by projecting the drivers onto PC axes and then using the main PC axes that explained the highest variance to regress against partitioned C fluxes to explain interannual variability in the growing season. In addition, we made use of environmental variability within each growing season by applying a conditional inference tree (Ctree) analysis (Hothorn et al., 2006) to determine the relationship of biweekly cumulative C fluxes (NEE, GPP, and $R_{\rm eco}$) with biweekly aggregated environmental variables (GDD, PAR, WTD, VPD, TD, T_S , Precipitation, and EVI) from April to September. Growing degree days was excluded from the $R_{\rm eco}$ model because it was derived from T_A that was also used to gapfill and determine daytime $R_{\rm eco}$. This model approach is a non-parametric class of regression models that preforms univariate splits on the dependent variables based on covariates. Unlike other classification regression tree models, Ctree does not overfit the models and are not biased toward covariates with many possible splits (Hothorn et al., 2006). Data were divided in two groups: a training set (80% original data set N = 153) and a test set (20%, N = 38) used to determine model performance. Analyses were performed using ctree function in partykit R package (Hothorn & Zeileis, 2015).

2.6. Uncertainty Analysis

Random error from gapfilling eddy covariance CO_2 flux measurements was characterized using the daily differencing approach (Hollinger & Richardson, 2005) with threshold of PAR \leq 75 (μ mol m⁻² s⁻¹), wind speed <1 m s⁻¹, and $T_A \leq 3$ °C (Figure S2). Uncertainties of the C flux components were assessed using a bootstrapping strategy (Liu et al., 2009); observations were fitted to the specified models and synthetic data sets were generated up to 1,000 values for each half-hourly NEE by randomly sampling on residuals. Models were fitted to the generated data sets and statistics applied. Error for the autochambers was reported as the standard error of the replicate chamber measurements, and so represents spatial differences in fluxes across the site.

3. Results

3.1. Environmental and Ecosystem Characteristics

The regional mean annual $T_{\rm A}$ has increased at a rate of 0.21°C per decade since 1925 (Figure 1), leading to a cumulative increase of 2.0°C over the 94-year measurement period (p < 0.0001). At the same time, a faster increase has been documented over the last 60 years; mean annual $T_{\rm A}$ increased at a rate of 0.45°C per decade (p < 0.0001) since 1959. Over the last 30 years, mean annual $T_{\rm A}$ increased at a rate of 0.68°C per decade (p = 0.006). Permafrost temperature measured in a borehole at the research site (Figure 2) indicated that ground temperature at different depths (below the depth of seasonal variation) increased since 1985 when the borehole was installed; ground temperature at 15 m depth increased from -1.26°C in 1989 to -0.76°C in 2018. Permafrost temperature increased sharply in the 1990s but levelled off during the first decade of the 2000s and the soil profile became isothermal. Renewed warming occurred in the last 5 years of the record and permafrost temperature at all depths matched or surpassed previous high temperatures recorded in the late 1990s.

Mean annual $T_{\rm A}$ for our study site was linearly related to mean annual $T_{\rm A}$ for the AKCD3 region, with the site having slightly but statistically higher temperatures on average (slope, p < 0.0001; intercept, p = 0.018; adjusted $r^2 = 0.88$). There was no statistical trend with time in mean annual $T_{\rm A}$ for the site-based measurement record during this study, probably due to the relatively short study period (2004–2018). Mean annual $T_{\rm A}$ at the study site during the 15 years of measurements was $-1.75^{\circ}{\rm C} \pm 1.52^{\circ}{\rm C}$ (Table 1). Permafrost is

SCHUUR ET AL. 6 of 23

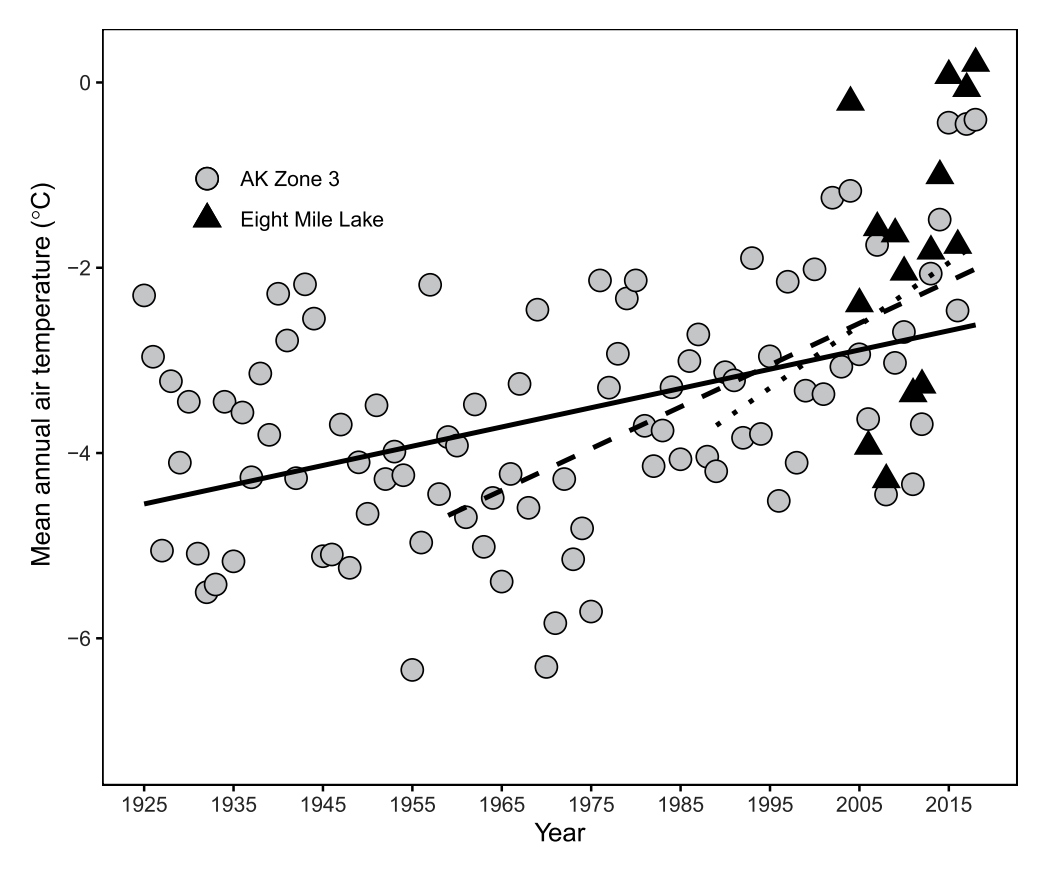


Figure 1. Mean annual air temperature for the NOAA AKCD3 region from 1925 to 2018, and for the Eight Mile Lake study site from 2004 to 2018. The solid line represents the average increase in temperature since 1925; dashed line since 1958; dotted line since 1989. All line fits are statistically significant and based on the AKCD3 data set. NOAA, National Oceanic and Atmospheric Administration.

generally sustained when mean annual $T_{\rm A}$ is consistently below zero. Notably, mean annual $T_{\rm A}$ in three of the last 4 years in the site temperature record was at or above zero, and 2018 was the warmest year on record. Based on the site temperature offset combined with the AKCD3 region measurements, these are likely to be the first years ever within the 94-year temperature record to exceed the zero-degree threshold.

The regional mean $T_{\rm A}$ in April exceeded the recent long-term mean (-3.64° C, calculated for the period 1971–2000) during 24 of the last 30 years (1989–2018). April mean $T_{\rm A}$ was above zero for eight of those 30 years, with anomalies reaching up to 5.5°C in 2007 and 2016 (Figure S3). Consequently, April mean $T_{\rm A}$ increased to -1.97° C calculated for the last 30 years. May and June have a similar pattern for mean $T_{\rm A}$. Mean $T_{\rm A}$ in October also exceeded the long-term mean (-5.8° C, calculated for the period 1971–2000) for most of the years of this study with anomalies greater than 6°C. This has increased the last 30 years (1989–2018) mean October $T_{\rm A}$ to -4.25° C. Growing degree-days followed patterns of $T_{\rm A}$, with the mean equal to $1510^{\circ} \pm 111^{\circ}$ (Table 1).

Soil temperature ($T_{\rm S}$) is controlled by a combination of incoming radiation and surface albedo, air temperature, snow depth in winter, soil moisture conditions, and other soil properties. Mean annual $T_{\rm S}$ at 10 cm depth at the site was $0.72^{\circ}\text{C} \pm 0.66^{\circ}\text{C}$ (2004–2018) (Table 1). Mean $T_{\rm S}$ for the growing season was $5.61^{\circ}\text{C} \pm 0.94^{\circ}\text{C}$, while the non-growing season mean $T_{\rm S}$ was $-3.54^{\circ}\text{C} \pm 1.72^{\circ}\text{C}$. Growing season precipitation during the study period was 245 ± 85 mm (Table 1) and varied almost three-fold from a low of 138 mm in 2013 to a high of 392 mm in 2016. Active layer thickness (ALT; Table 1), the deepest thaw reached during the growing season, was on average 66.0 ± 3.5 cm ranging from 59.4 cm in 2011 to 71.8 cm in 2018.

The enhanced vegetation index (EVI), varied between 0.3 and 0.5 between June to August over the study period (Figure 3). However, the beginning of plant activity as defined by EVI varied by at least 6 weeks

SCHUUR ET AL. 7 of 23

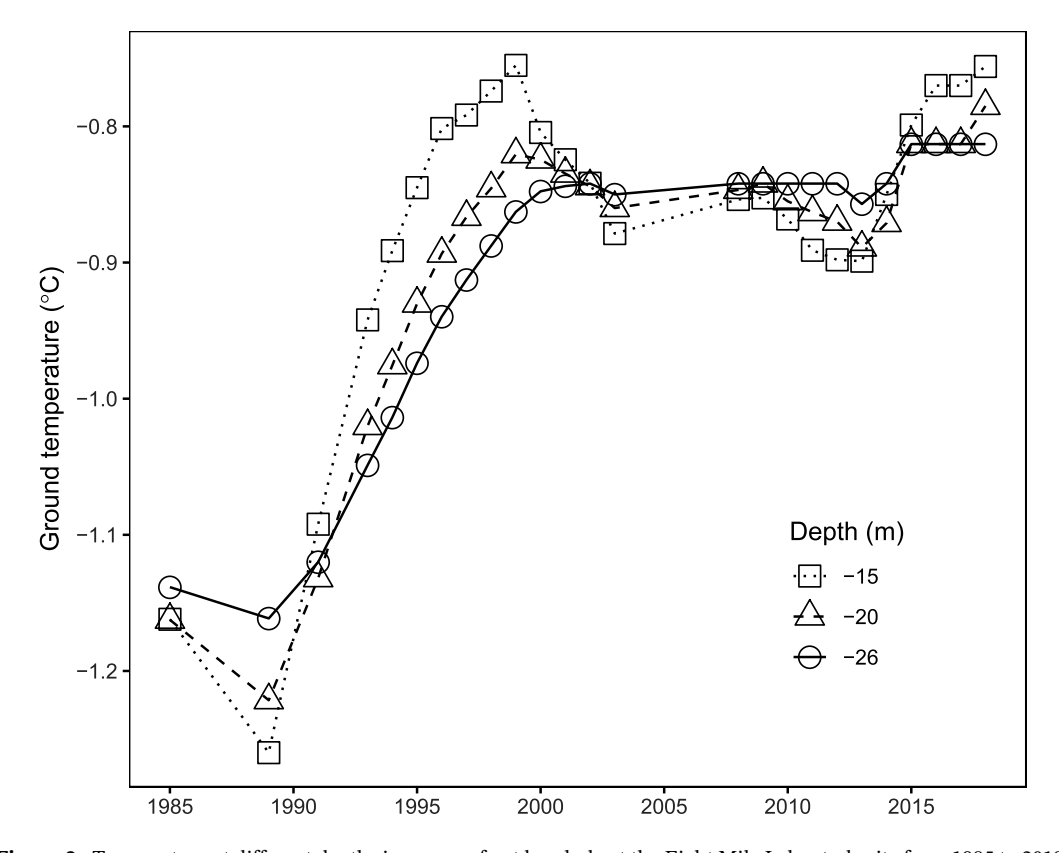


Figure 2. Temperature at different depths in a permafrost borehole at the Eight Mile Lake study site from 1985 to 2018. Measurement depths are located below the depth influenced by seasonal temperature variation.

across the 15 years of study. For example, EVI reached a similar value (\sim 0.15) in early April 2016 and in late May in 2013; the latter year was characterized by deep snowpack and a cool spring. The end of plant activity, as defined by EVI, also varied by at least 6 weeks across the study period; it was near or below 0.1 in early September in 2004 and 2015, and was still 0.17 at end of October in 2016. Variation in biweekly EVI across the entire 15-year record was driven by the thermal stage of the ecosystem: GDD and T_S (Figure S4).

3.2. Carbon Fluxes

The tundra ecosystem was on average a C source to the atmosphere across the 15 years of study (Figure 4; Table S1a). Mean annual NEE was 52.5 ± 55.5 g C m⁻² yr⁻¹, varying from a C sink of -70.0 g C m⁻² yr⁻¹ in 2015 to a C source of 138.4 g C m⁻² yr⁻¹ in 2014. The ecosystem released a cumulative 781.6 g C m⁻² over the 15 years of study. Mean annual GPP (Figure 4; Table S1b) was -441.3 ± 101.4 g C m⁻² yr⁻¹; GPP varied almost three-fold, from -275.8 g C m⁻² yr⁻¹ in 2005 to -726.8 g C m⁻² yr⁻¹ in 2015. Chamber and eddy covariance C fluxes measured simultaneously in 2008 gave almost exactly the same annual GPP estimate. Mean annual $R_{\rm eco}$ was 495.3 \pm 80.5 g C m⁻² yr⁻¹ (Figure 4; Table S1c); $R_{\rm eco}$ varied by a factor less than two, from 388.6 g C m⁻² yr⁻¹ in 2005 to 656.8 g C m⁻² yr⁻¹ in 2015. NEE did not show a uniform directional trend over the 15 years of study; however, GPP decreased (greater magnitude on negative scale) at a rate of 13.9 g $C \text{ m}^{-2} \text{ yr}^{-1}$ (p = 0.005), while R_{eco} increased at 13.5 g C m⁻² yr⁻¹ (p = 0.0002). The absolute slope values of GPP and R_{eco} were not significantly different (p = 0.95). These statistical relationships for GPP and R_{eco} were not significant using the shorter eddy covariance record alone (2008-2018), but this could be the effect of a shorter time series on regression statistics. We found no evidence from co-occurring measurements in 2008, or in another chamber versus eddy covariance analysis from the site using multiple years of data (Celis et al., 2017), to suggest that ecosystem C exchange should not be analyzed across the full time series while at the same time keeping the different methodologies in mind.

SCHUUR ET AL. 8 of 23

Table 1

			T. (°C)				(הי) תתם				$T_{c}(^{0}C)$			Precip (mm)	ALT (cm)
			14(5)								(2) (2)				
P year	April	CS	October	Non_GS	Annual	April	GS	October	April	CS	October	Non_GS	Annual	CS	End or GS
2004	0.14	11.27	-1.41	-11.50	-0.14	45.11	1756.06	27.55	NA	6.40	-0.13	-2.16	1.87	153.2	61.5
2005	-0.67	10.53	-4.28	-15.35	-2.36	69.17	1615.36	14.93	-2.13	6.71	-0.62	-6.58	-0.14	145.1	9.89
2006	-3.51	9.43	-3.08	-17.43	-3.81	7.55	1445.86	50.81	-4.41	6.27	NA	-6.75	-0.51	227.4	61.9
2007	2.54	10.26	-7.36	-13.04	-1.54	79.41	1570.13	2.27	-2.83	7.09	-0.35	-3.85	1.10	331.3	0.89
2008	-4.22	8.14	-10.40	-15.57	-4.25	31.05	1270.85	4.25	-2.19	5.11	-0.14	-3.15	9.02	346.2	67.8
2009	-2.17	9.71	-1.41	-12.93	-1.58	44.24	1520.07	64.53	-3.67	6.12	0.16	-6.09	-0.24	178.2	66.1
2010	1.22	9.84	-3.08	-14.38	-2.01	62.31	1542.18	31.25	-2.10	09.9	-0.31	-4.25	0.80	249.8	0.69
2011	-2.58	9.45	-2.55	-16.58	-3.38	32.05	1451.81	26.90	-3.30	5.40	-0.15	-3.56	0.50	164.4	59.4
2012	-0.05	9.14	-7.14	-15.55	-3.21	56.48	1422.20	30.93	-1.46	00.9	90.0	-1.65	1.71	223.4	64.4
2013	-11.29	9.27	1.43	-11.58	-1.71	0.00	1517.78	75.05	-1.92	4.73	0.22	-1.91	1.06	137.8	65.2
2014	-0.86	9.14	-7.94	-9.76	-0.95	60.55	1404.31	0.18	-1.53	4.95	-0.37	-2.77	0.77	312.2	62.8
2015	0.15	9.52	-1.56	-9.08	0.09	42.14	1478.13	23.38	-0.83	4.71	-0.19	-3.33	0.50	354.4	65.0
2016	2.91	10.29	-2.18	-14.71	-1.72	94.17	1575.61	51.85	-0.05	5.75	-0.35	-3.35	0.99	392.4	70.3
2017	-0.35	10.42	-1.48	-10.17	0.00	35.39	1595.23	48.30	-2.09	4.03	0.32	-1.35	0.98	187.2	0.89
2018	-3.51	99.6	1.59	-8.85	0.26	12.87	1485.32	103.50	-0.76	4.93	09.0	-2.42	0.80	265.0	71.8
Mean ± sd	-1.48 ± 3.44	9.74 ± 0.74	-3.39 ± 3.44	Mean \pm sd $$ -1.48 \pm 3.44 9.74 \pm 0.74 \pm 3.39 \pm 3.44 -13.10 \pm 2.82	Ϊ	44.83 ± 26.43	3 1510 ± 111	$1.75 \pm 1.52\ 44.83 \pm 26.43\ 1510 \pm 111\ 37.05 \pm 28.95 - 1.97 \pm 1.24\ 5.61 \pm 0.94 - 0.09 \pm 0.33 - 3.54 \pm 1.72\ 0.72 \pm 0.66\ 244.5 \pm 85.1\ 66.0 \pm 3.59 \pm 0.39 \pm 0.3$	-1.97 ± 1.24	5.61 ± 0.94	-0.09 ± 0.33	-3.54 ± 1.72	0.72 ± 0.66	244.5 ± 85.1	66.0 ± 3.5

Note. Spring transition month, April, growing season (GS, May 1 to September 30); fall transition month, October; non-growing season (Non_GS, November 1 to March 31 following calendar year).

SCHUUR ET AL. 9 of 23

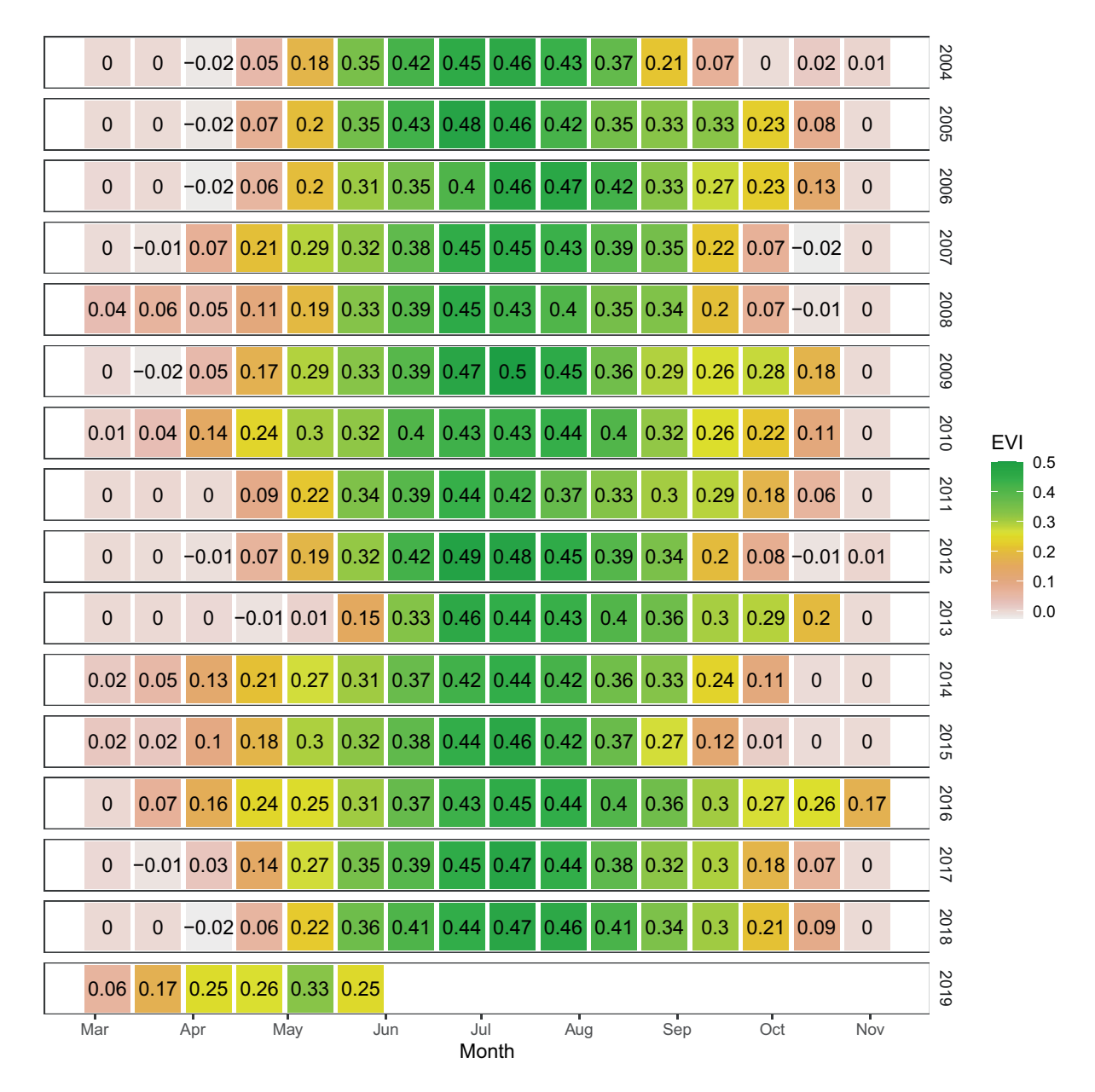


Figure 3. Biweekly Enhanced Vegetation Index (EVI) from the MODIS EVI product retrieved over the Eight Mile Lake study site.

Mean growing season NEE was -98.2 ± 41.9 g C m⁻² season⁻¹ and was always a C sink, ranging six-fold from -35.1 g C m⁻² season⁻¹ in 2005 to -200.7 g C m⁻² season⁻¹ in 2015 (Table S1a; Figure S5). Transition months (April and October) were net C sources all years. June and July were the months with highest NEE with June 2015 having had a net C uptake extreme that was greater than -80 g C m⁻² month⁻¹. Mean growing season GPP was -431.7 ± 91.2 g C m⁻² season⁻¹ (Table S1b; Figure S5), ranging more than two-fold from -275.8 g C m⁻² season⁻¹ in 2005 to -678.6 g C m⁻² season⁻¹ in 2015. The ecosystem had detectable GPP in April for all years that NEE was measured (no data was available in the early chamber years in the record). Maximum GPP generally occurred in June and July (July mean greater than -125 g C m⁻² month⁻¹). GPP was generally very low in October, and it usually was detectable only during the first week of the month. Mean growing season R_{eco} was 333.5 ± 68.1 g C m⁻² season⁻¹ (Table S1c; Figure S5). R_{eco} always exceeded GPP in spring (April) and fall (September-October) driving the ecosystem towards being a C source, but with June, July, and August being the months with the highest absolute mean R_{eco} . Mean non-growing season R_{eco} was 102.3 \pm 20.7 g C m⁻² season⁻¹ (Table S1c; Figure S6), varying from 81.6 g C m⁻² season⁻¹

SCHUUR ET AL. 10 of 23

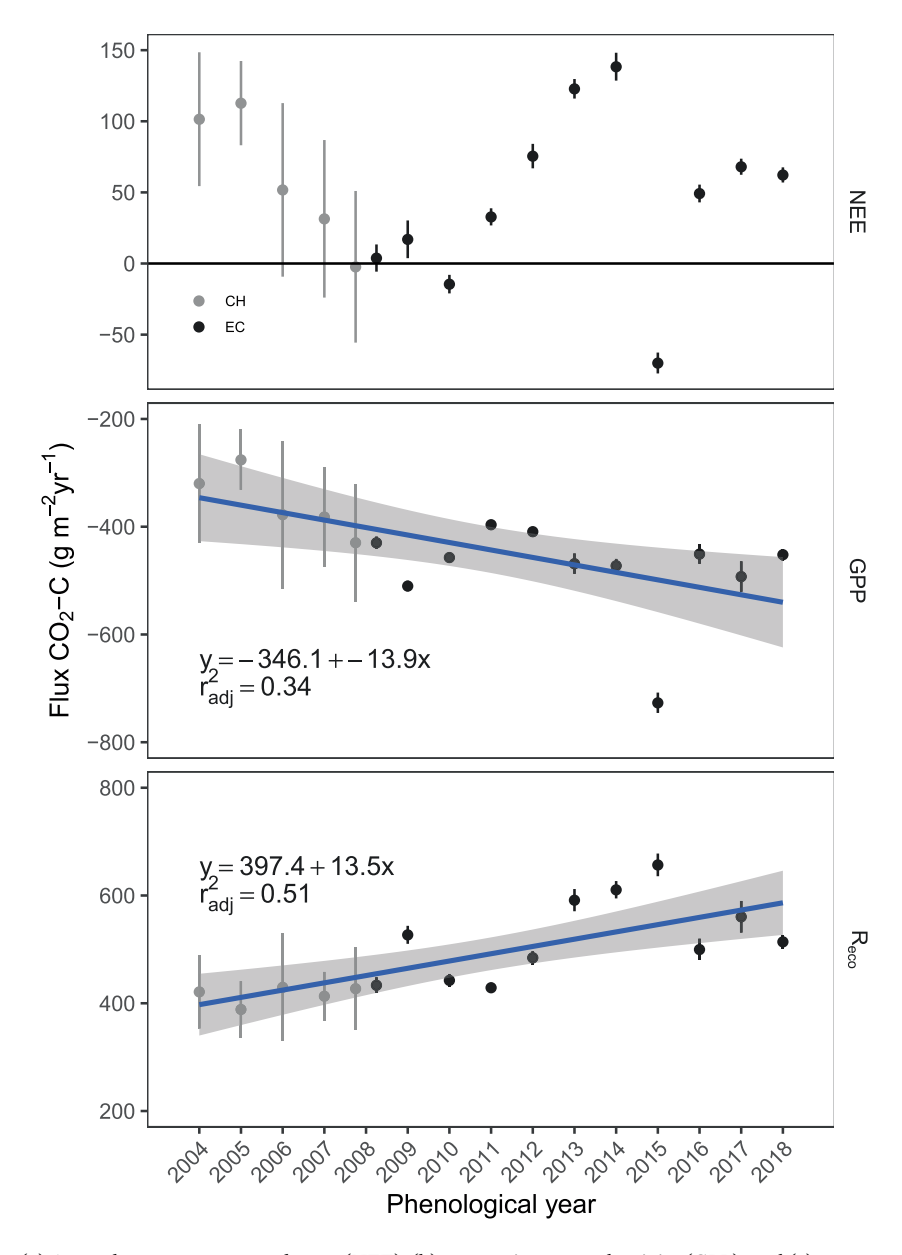


Figure 4. (a) Annual net ecosystem exchange (NEE), (b) gross primary productivity (GPP), and (c) ecosystem respiration ($R_{\rm eco}$) from 2004 to 2018 at the Eight Mile Lake study site. Chamber measurements (CH) shown in grey; eddy covariance (EC) measurements in black. Error bars for individual years are described in more detail in the main text and represent spatial error for the chamber measurements, and bootstrapped gapfilling error for the single eddy covariance tower. The regression line (blue) and associated standard error of the slope (grey shading) is based on the mean carbon flux estimate for each year across the 15-year record.

in 2010 to 162.8 g C m⁻² season⁻¹ in 2014. On average, the growing season accounted for 67% of the annual $R_{\rm eco}$, mean non-growing season $R_{\rm eco}$ accounted for 21% of annual $R_{\rm eco}$, while the transition months of April and October accounted for 12% of the annual $R_{\rm eco}$.

The period of plant activity, as measured here by the first and last day when GPP was detectable (Table S2), was on average 154 ± 18 days. The longest period (196 days in 2015) was 27% longer than the mean; it extended from March 26 all the way to the end of the first week of October. In contrast, the shortest period (126 days in 2013) was 18% shorter than the mean, extending from May 28 to the first day of October driven primarily by the delayed spring.

SCHUUR ET AL. 11 of 23

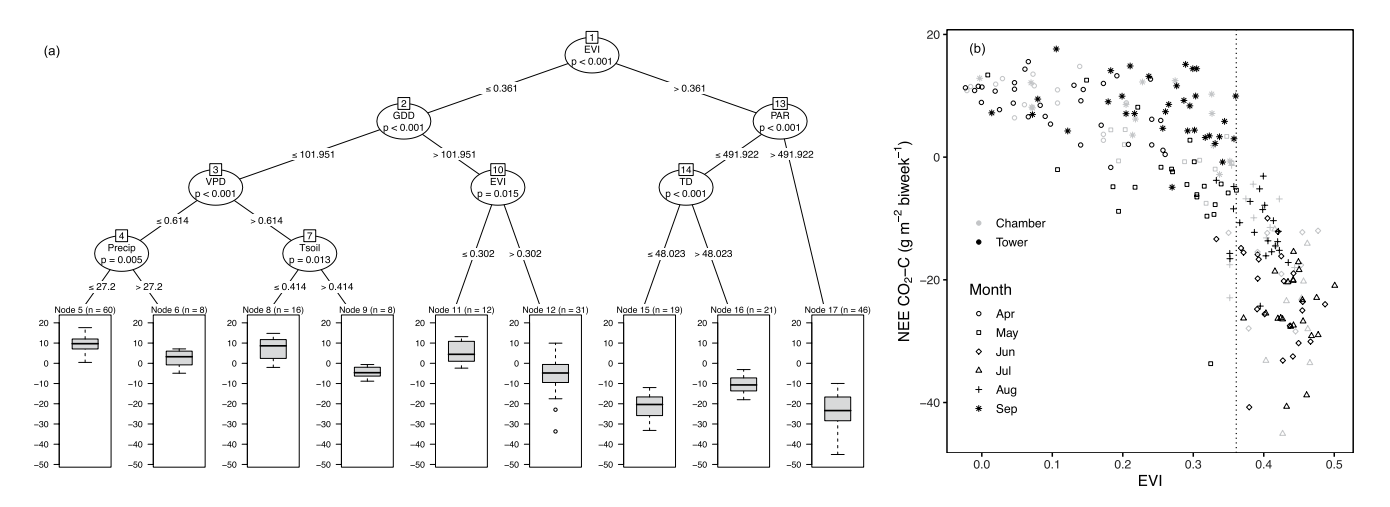


Figure 5. (a) Conditional regression tree for biweekly aggregated net ecosystem exchange (NEE) during the growing season using environmental variables and enhanced vegetation index (EVI); box plots show NEE data distribution grouped at each node. (b) The relationship of biweekly NEE versus biweekly EVI, at the Eight Mile Lake study site. The dashed line shows the *x*-axis value that defines the first node in the regression tree.

3.3. Drivers of Carbon Flux

Interannual variability in annual $R_{\rm eco}$ was positively related to mean $T_{\rm A}$ ($y=539.1+35.7^*T_{\rm A}$, $r^2=0.27$, p=0.04), whereas variability in annual NEE and GPP were not significantly related to mean $T_{\rm A}$ or mean $T_{\rm S}$. Non-independent correlations between annual NEE and growing season (r=0.94, p<0.001) and non-growing season (r=0.48, p=0.056) NEE suggested that factors controlling C dynamics during the growing season period had the larger impact on annual NEE, in part because fluxes were larger overall during the growing season.

For the growing season, a principal component (PC) analysis indicated that climate and site environmental drivers projected on the first two component axes explained 71.9% of the environmental variance across years (Figure S7, Table S3a). Of the two PC axes, GPP was significantly correlated to PC1 ($r^2 = 0.32$ p = 0.021), as was $R_{\rm eco}$ ($r^2 = 0.35$, p = 0.016; Table S3b). This PC1 axis explained a similar amount of environmental variance (38.4%) in comparison to the PC2 axis (33.5%), with PC1 having a negative correlation with $T_{\rm S}$ as the strongest single variable, followed by positive correlations with PAR and WTD, and negative correlations with VPD and TD (Table S3a). These correlations indicated that growing season C uptake from GPP and loss from R_{eco} generally were larger when the surface soil was cooler and overall total soil thaw was shallower, when there was more light, and when air and soils were wetter. NEE was not significantly correlated with either PC axis, but showed more of a trend with the PC2 axis (p = 0.12). The PC2 axis shared many similar variables as PC1 but with some contrasts. The strongest single variable for PC2 was a negative correlation with precipitation followed by negative correlations with EVI and TD. These variables were followed in strength by a negative correlation with WTD, and positive correlations with PAR and VPD (Table S3a). These correlations indicated generally (but not significantly) higher NEE when there was lower rainfall, lower leaf area/activity, and overall shallower soil thaw, along with drier air and soil, and more light; NEE being a composite measure having higher values with higher Reco and/or lower GPP and lower values when the opposite pattern is true.

Conditional regression tree models were used to determine environmental controls over biweekly variability in growing season C exchange. For biweekly NEE, EVI was the most important factor driving variation (Figure 5, node 1). The regression tree split at EVI equal to 0.36; below this value (conditions with lower leaf area), GDD became the most important factor. With lower GDD (cool conditions), a combination of VPD, precipitation and T_S controlled biweekly NEE. These conditions corresponded to the months of April–May when conditions were warming up in the early season, and also included September when air temperatures were cooling down at the end of the season (Figure 5b). In these cooler and drier periods with low leaf area/activity, the ecosystem was generally a C source (Figure 5, nodes 3,4,7) except when VPD >0.6 kpa (more moisture) and T_S was greater than 0.4°C (warmer soil; Figure 5, node 7). When leaf area/activity was higher

SCHUUR ET AL. 12 of 23

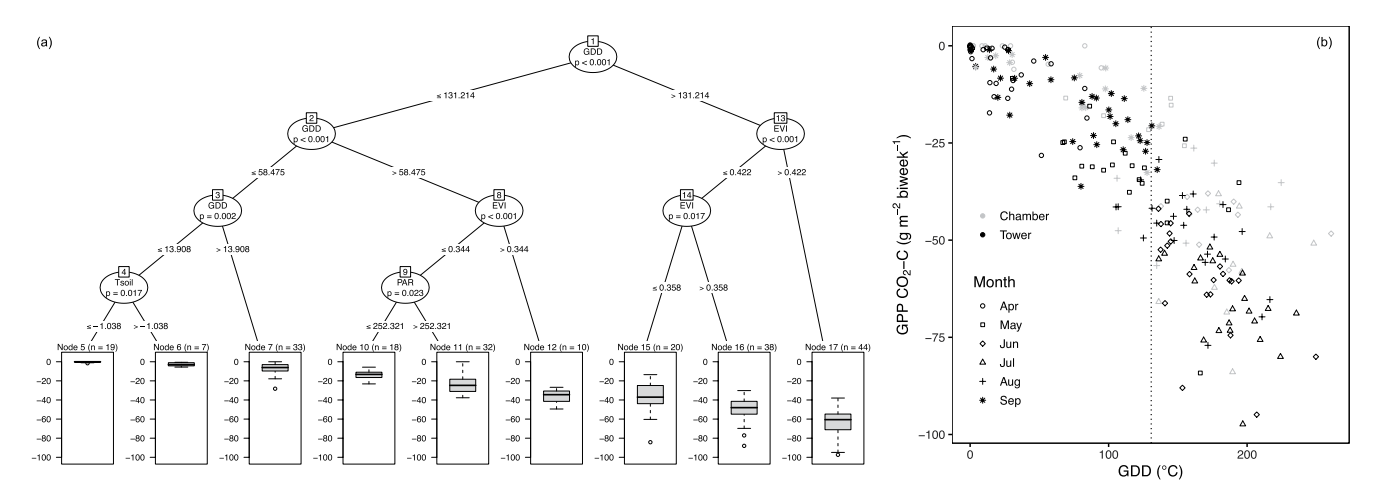


Figure 6. (a) Conditional regression tree for biweekly aggregated gross ecosystem exchange (GPP) from environmental and enhanced vegetation index (EVI); box plots show GPP data distribution grouped at each node. (b) The relationship of biweekly-integrated GPP versus aggregated growing degree-days (GDD) at the Eight Mile Lake study site. The dashed line shows the *x*-axis value that defines the first node in the regression tree.

(Figure 5, node 1,10), the ecosystem was a C sink, a tendency further stimulated by higher light (Figure 5, node 13). When leaf area/activity was high and light was lower, the C sink was reduced when TD was also high (Figure 5, node 14).

For biweekly GPP, there were generally a similar set of environmental factors that explained variation. The regression tree split first at GDD equal to cumulative 131°C (Figure 6, node 1). A second split with GDD occurred in cooler conditions (Figure 6, node 2), with $T_{\rm S}$ dictating the level of C uptake in the coolest conditions (Figure 6, node 4), and EVI and PAR dictating the level of C uptake in the warmer part of this branch of the regression tree (Figure 6, node 8, 9). In warmer conditions in the peak of the growing season June-August (Figure 6b; GDD > cumulative 131°C), EVI alone dictated the level of C uptake.

When the same variable set was used in the biweekly $R_{\rm eco}$ regression tree, then GDD also assumed dominance as the driving variable across the entire regression tree with $T_{\rm S}$ as the only other environmental variable playing a role (data not shown), but with the caveat that air temperature had already been used to help produce the biweekly $R_{\rm eco}$ values. When GDD was removed from the analysis, EVI level defined the first regression tree split (Figure 7, node 1). In conditions with lower leaf area, lower $T_{\rm S}$ (cooler conditions) decreased biweekly $R_{\rm eco}$ (Figure 7, node 2, 3). When leaf area was higher, then the level of leaf area and VPD controlled biweekly $R_{\rm eco}$ (Figure 7, node 7, 8), with drier conditions reducing respiration.

4. Discussion

4.1. Carbon Flux and Environmental Change through Time

The tundra ecosystem at the Eight Mile Lake research site where permafrost is degrading was a net source of CO_2 -C to the atmosphere at a rate of 52.2 g C m⁻² yr⁻¹, for a cumulative total loss of 781.6 g C m⁻² over the 15-years study period (Figure 4). Over time, there was a linear increase in plant C uptake (GPP) and a corresponding linear increase in ecosystem C release (R_{eco}), but the slopes of these trends were not statistically different from one another and so together there was no single trend through time for net C exchange (NEE). Similarly, there was no air temperature trend through time using our 15-year site record, but comparing our record to the longer Interior Alaska air temperature record revealed interesting insights (Figure 1). In the regional record, air temperature trends were not statistically significant over shorter (15-year) periods but were over longer time periods, due to the statistical effects of interannual variability. The regional record indicated that the site has warmed by 2°C since 1925. This rate of warming has more than tripled recently; the regional rate for the most recent 30 years was 0.68°C decade⁻¹, which is also consistent with temperature trends compiled for the Arctic region as a whole (Overland et al., 2017). While our site air temperature records were too short to detect trends over time, we did record novel conditions that are likely unmatched over the last century. The last three years at the site were at, or above, 0°C, the long-term

SCHUUR ET AL. 13 of 23

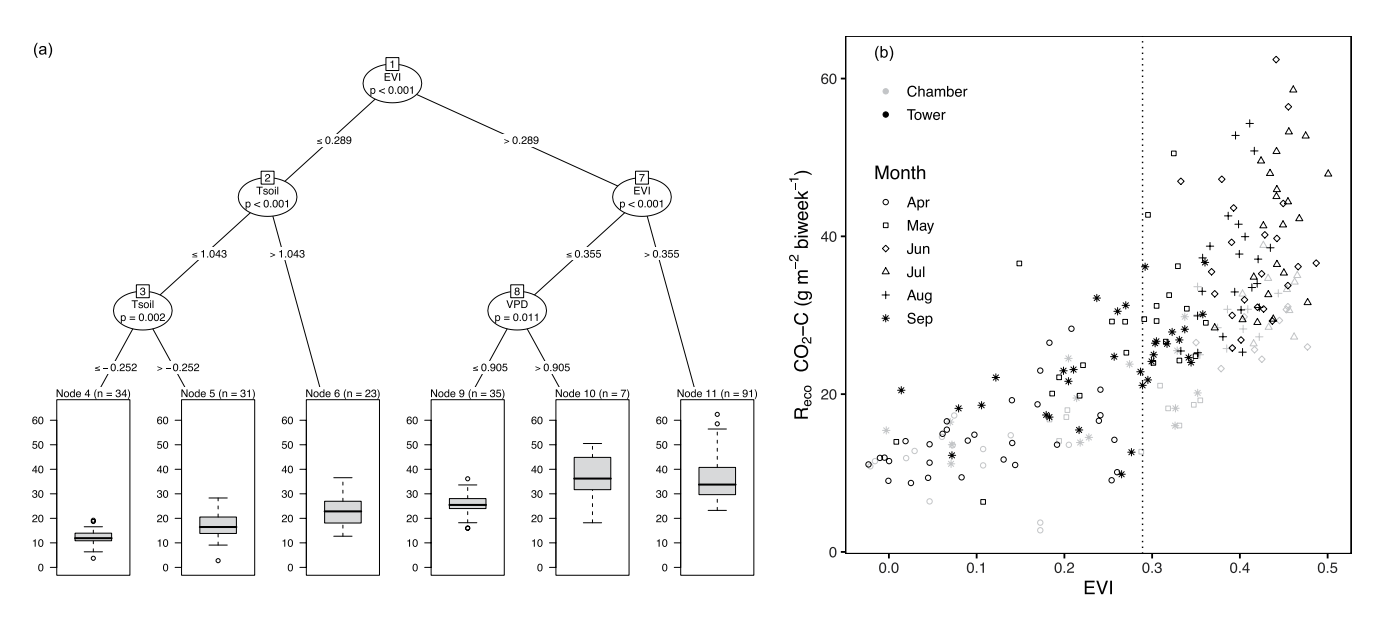


Figure 7. (a) Conditional regression tree for biweekly aggregated ecosystem respiration (R_{eco}) from environmental and enhanced vegetation index (EVI); box plots show R_{eco} data distribution grouped at each node. (b) The relationship of biweekly-integrated R_{eco} versus biweekly EVI at the Eight Mile Lake study site. The dashed line shows the *x*-axis value that defines the first node in the regression tree.

mean annual air temperature required to sustain permafrost. In addition, a warming anomaly of 4.7° C was registered across Alaska for the winter of 2015/2016 (El Niño conditions), and climate simulation models indicate that air temperatures at the level of this anomaly may become the new average by 2050 (Walsh et al., 2017). These temperature trends for the Arctic region are forecasted to continue, reaching $>8^{\circ}$ C by 2100 above a 1986-2005 baseline if no attempts to reduce anthropogenic greenhouse gas emissions are made (IPCC, 2013; Overland et al., 2014). While there were no linear NEE trends with time in our 15-year record, the documented novel climate conditions and long-term warming trends are an important backdrop to the C cycle dynamics observed at the site.

4.2. Seasonal Drivers of Net Carbon Loss and Gain

In our 15-year record, the ecosystem was an annual CO₂ source (mean NEE was positive) for 13 of the years, and an annual CO₂ sink (mean NEE was negative) for only two of the years (Figure 4, Table S1a). Focusing on the years where NEE was at least one standard deviation (SD) higher or lower than the 15-year mean exchange (7 out of 15 years) provides insight into the patterns of C source/sink dynamics that can help understand the possible future of this ecosystem. The top two years in absolute magnitude were C sources (2014, 2013) when GPP was near average, but $R_{\rm eco}$ was at least one SD higher than the mean, with 2014 having notably higher C release in the non-growing season as well (Tables S1a, S1b, and S1c). The top C sink year (2015) that tied in magnitude (but opposite direction) with the second highest C source year (2013) was when all biological processes were stimulated by at least one SD, but GPP even more so than $R_{\rm eco}$ including an early season start with relatively large uptake in April. The years with next largest magnitude were again C sources (2005, 2004) where biological processes were generally suppressed, but GPP was depressed more than $R_{\rm eco}$. The two lowest years for net summer C uptake were 2005 and 2013, which helped lead to high annual C source years. Finally, when GPP was average, the ecosystem was either a small C sink (2010) when $R_{\rm eco}$ was below average, or near neutral (2008) when $R_{\rm eco}$ was average. These final two years were not storing much ecosystem C as compared to 2015, but did slow the loss as compared to the 15-year average. Taken together, the ecosystem was only a significant C sink when GPP was exceptionally high relative to the average; it could be a small C sink when GPP was average, only if $R_{\rm eco}$ was lower than average. Under most other diverse conditions, R_{eco} losses overwhelmed GPP gains such that the ecosystem was an annual net C source.

The seven-month period including the non-growing season (November–March) and the transition months (April, October) plays a secondary, yet still important, role in the site losing net CO₂ on an annual basis

SCHUUR ET AL. 14 of 23



(Tables S1a, S1b, and S1c). This period contributed an additional 50% to the annual $R_{\rm eco}$ as compared to growing season $R_{\rm eco}$ alone, with almost two-thirds of that released during the non-growing season and the remainder of the release occurring in April and October equally. Properly accounting for these additional ecosystem C losses offsets better documented net C uptake during the growing season and can shift tundra ecosystems into annual net C sources (Belshe et al., 2013; Natali et al., 2019; Oechel et al., 2014; Webb et al., 2016). Eddy covariance estimates of non-growing season C fluxes tend to be higher than chamber-based estimates (Natali et al., 2019; Webb et al., 2016); this might be linked to winter respiration losses that can pulse release through cracks in frozen ground (Raz-Yaseef et al., 2017), and are thus difficult to quantify with small chamber bases and infrequent manual sampling. The non-growing season time series is too short within this study, and the data are overall too scarce elsewhere (Belshe et al., 2013; Natali et al., 2019) to determine if non-growing season C fluxes were larger than they once had been. There were no trends through time with our non-growing season C fluxes, and six of the top seven years with either high or low annual NEE had non-growing season C fluxes that were near the average. At the same time, observed mean annual Arctic temperature increase has been largely driven by warmer temperatures in fall and winter (Overland et al., 2014), and this should have a direct effect on R_{eco} outside of the growing season, which is often gap filled based on air or soil temperatures, among other variables.

The transition months of April and October represent net C sources in all years of our record, but they also represent the months where detectable GPP started and ended. The start of plant activity varied with a range of almost two months, in contrast to the end of plant activity, which varied within a 2-week range (Tables S1a, S1b, and S1c, Table S2). This difference in start of season variability in GPP was matched by the remotely-sensed leaf area/activity index, whereas EVI was equally variable (by several months) at the end of season as well (Figure 3). This had an impact on C fluxes: there was a correlation between start/end date and GPP in both April and October ($r^2 = 0.82$, p < 0.05; $r^2 = 0.68$, p < 0.05), although this was closely related to how start/end date was defined. But in April, start/end date was also correlated to NEE ($r^2 = 0.57$, p < 0.05), which varied by a factor of 13 across years, but not in October ($r^2 = 0.14$, p > 0.05) where NEE only varied by a factor less than 2. In summary, both months contributed a similar amount of net C to the atmosphere on average (~25 g C m⁻² NEE) but variation in the timing of plant C uptake in April had a much stronger control over the contribution of C by this spring transition month to the annual total as compared to October, where levels were more consistent across years. Based on the regional temperature trends, both of these months were consistently much warmer during our 15-year observation period than they once were (Figure S3), but the effect of these months alone on total C exchange were modulated by environmental differences in other seasons as well (Parmentier et al., 2011).

4.3. Mechanisms Controlling Carbon Fluxes

Over historical times, the Eight Mile Lake tundra ecosystem has been a net C sink (GPP > R_{eco}) for atmospheric CO₂ (Harden et al., 1992; Shaver et al., 2000), accumulating 180-360 g C m⁻² in aboveground plant biomass (Hewitt et al., 2019; Salmon et al., 2016; Schuur et al., 2007) with another 600 g C m⁻² in belowground plant biomass (Hewitt et al., 2019), and 55-69 kg C m⁻² soil organic matter in the top 1 m (Pries et al., 2012). For this tundra site to have become a consistent C source to the atmosphere in recent times, GPP would have either: (1) decreased while R_{eco} stayed the same; (2) stayed the same while R_{eco} increased, or (3) increased but with $R_{\rm eco}$ having increased faster. The 15-year time series points towards the third possibility but doesn't show that $R_{\rm eco}$ is currently increasing faster than GPP, indicating that $R_{\rm eco}$ increases must have been greater than GPP increases prior to 2004 (Figure 4). This is consistent with the earlier timing of the permafrost borehole temperature increases (Figure 2), the long-term air warming trends from the regional record (Figure 1), and the significant relationship between annual $R_{\rm eco}$ (but not GPP) and annual air temperature from our record. At the same time, atmospheric CO₂ rose 30 ppm over our 15-year time series to 400 ppm in the summer of 2018 (NOAA., 2019). Over this time, GPP increased by a cumulative 210 g C m⁻² yr⁻¹. This 66% increase is well beyond the stimulation rate of mature ecosystems exposed to elevated CO₂ (DOE, 2020; Jiang et al., 2020), and thus likely reflects multiple environmental mechanisms operating to enhance GPP in addition to CO2 fertilization, such as increased nutrient availability, warmer temperatures and longer growing seasons. Taken together, while GPP and $R_{\rm eco}$ are both likely to have increased from historical rates and do so in the measurement record, the consistent C source observations suggest that GPP increases did not match those of R_{eco} .

SCHUUR ET AL. 15 of 23



Correlations between environmental and ecosystem factors, as described by PC axes, and interannual variation in C exchange during the growing season helps to understand how GPP and Reco may continue to respond in the future across years (Figure S7, Tables S3a and S3b). Growing season C uptake by GPP and loss by $R_{\rm eco}$ were both larger when surface soil was cooler and overall total soil thaw was shallower, when there were higher light levels, and when air and soils were wetter. This highlights not only the role of temperature but also of moisture that plays a role in controlling both plant and microbial activity (Keuper et al., 2012; Yuan et al., 2019). In fact, cooler surface soil and shallower thaw depth may also be a proxy for wetter conditions, since temperature generally has a positive effect on plants and soils (Davidson & Janssens, 2006; Grant et al., 2011; Kirschbaum, 2000; Rustad et al., 2001), whereas this analysis showed the reverse correlation with GPP and Reco. These environmental correlations also indicated generally (but not significantly) higher growing season NEE (increased C source) when there was lower rainfall, lower leaf area/activity, and overall more shallow depth soil thaw, along with drier air and soil, and increased light levels. Again, the influence of drier conditions (air, soil, precipitation, and more light/less clouds) to increase NEE suggests that water limitation of plant growth is stronger than the effect of moisture on microbial activity. This is consistent with the presence of perched water within the soil profile sitting at the thaw surface, potentially providing a source of water to soil processes (Mauritz et al., 2017; Natali et al., 2015; Pries et al., 2013), whereas shallowly-rooted tundra plant species (Hewitt et al., 2019) and non-vascular mosses and lichens at the soil surface are likely to be more dependent on precipitation inputs and humidity.

Correlations between short-term (biweekly) site and environmental and ecosystem variables and $R_{\rm eco}$ within the growing season as determined by regression tree analysis demonstrated the shifting dominance of plants and soil microbes on C release from early to late in the growing season (Figure 7). Across the season, GDD stimulated GPP, $R_{\rm eco}$, and EVI, along with soil temperature, pointing to the well-known dominant effect of warm temperatures to stimulate biological processes (Davidson & Janssens, 2006). Leaf area/activity was a strong control over GPP and also R_{eco} , at least when GDD was removed from the latter analysis. In contrast to controls over interannual variability in growing-season GPP, moisture did not show up as a direct control over biweekly GPP, but it could be that moisture affected leaf area/activity, which itself had a stronger control over short-term GPP (Figure 6). In the peak growing season when leaf area/activity was high, biweekly NEE was higher with more light, which stimulated plant C uptake, but was depressed by increased thaw depth when more soil C was exposed to decomposition and microbial respiration offset, in part, C uptake by plants (Figure 5). Of these two variables, light is primarily controlled by season with cloudiness playing a secondary role; future changes in light seem more constrained and any increases (more light/less clouds) could be linked to drier conditions, which itself has a negative effect on NEE in the interannual analysis. In contrast, the exposure of more soil C with increased thaw depth seems to have more potential to change with future warmer conditions as compared to light, which would tend to favor ecosystem C losses over C gains. Lastly, when conditions were cool in the early and late season, biweekly NEE was often a C source. It was in these conditions where moisture (VPD, precipitation) played the clearest role along with temperature. For the most part, short-term controls over GPP, R_{eco} , and NEE were consistent with interannual variability in growing season C fluxes, demonstrating the strong influence of temperature (Parmentier et al., 2011) and also, importantly, moisture in controlling the within-season interplay between plant and microbial controls over C fluxes.

4.4. Net Carbon Loss in the Tundra Biome

Eight Mile Lake is currently a sustained source of CO_2 to the atmosphere linked to warming temperatures and thawing permafrost, and this pattern is becoming more common across the region. Recent syntheses of ecosystem CO_2 fluxes have alternately reported tundra ecosystems as C sinks or neutral averaged across the circumpolar region for the 1990s and 2000s (McGuire et al., 2012), or C sources over the same time period (Belshe et al., 2013). Across the Arctic for upland tundra, Belshe et al. (2013) estimated that annual net C loss averaged 21–36 g C m⁻² yr⁻¹ between the years 2002 and 2010; sites with higher mean annual air temperature, for example near 0°C similar to recent Eight Mile Lake conditions, had generally higher loss rates at or above 50 g C m⁻² yr⁻¹. Similar to the Eight Mile Lake time series, both syntheses agreed that the summer growing season is a period of net C uptake into terrestrial ecosystems, and this uptake appears to be increasing as a function of vegetation density/biomass (Ueyama et al., 2013). The discrepancy between these syntheses may be a result of CO_2 release rates during the non-summer season that are now thought to

SCHUUR ET AL. 16 of 23



be higher than previously estimated. The latest synthesized October to April CO $_2$ release rates ranged from 20 to 40 g C m $^{-2}$ for the coldest sites in the permafrost region up to 180 to >200 g C m $^{-2}$ for the warmest sites (Natali et al., 2019). For context, Eight Mile Lake CO $_2$ release averaged ~150 g C m $^{-2}$ between October to April, whereas the more limited winter data synthesized earlier was estimated to range only from 30 to 40 g C m $^{-2}$ across different Arctic continental regions (McGuire et al., 2012).

The other explanation for the source/sink difference between Belshe et al. (2013) and McGuire et al. (2012) is the separation of upland and wetland ecosystem types, which was done in the former synthesis (uplands only) but not the latter (both combined). In fact, comparing the limited data by upland and wetland ecosystem types revealed that uplands like Eight Mile Lake were annual net C sources whereas wetlands were annual net C sinks (McGuire et al., 2012), although all sites were combined for the regional upscaling described earlier. Soil moisture status, especially anaerobic conditions, is a primary control over ecosystem C sink/source strength with wetlands more often than not still acting as annual net C sinks even while $\rm CH_4$ is emitted (Boelman et al., 2003; Euskirchen et al., 2014; Lund et al., 2010). Even so, recent long-term measurements on the North Slope of Alaska have shown both dry (heath) and wet (wet sedge, tussock) tundra ecosystems to be releasing net $\rm CO_2$ to the atmosphere in the most recent decade (Euskirchen et al., 2017), suggesting that protection of soil organic matter by anaerobic processes, in addition to cold temperatures, may also be undergoing change.

Recent aircraft measurements of atmospheric CO_2 concentrations over Alaska also showed that tundra regions of Alaska were a consistent net CO_2 source to the atmosphere for the period 2012–2014 (Commane et al., 2017), which would include both upland and wetland ecosystem types (Lara et al., 2018). The aircraft study region as a whole, which included tundra on the North Slope of Alaska as well as South West Alaska, was estimated to be a net C source of 22.7 Tg CO_2 -C year⁻¹ averaged over the land area of both regions for the entire study period. The aircraft-based estimate of net release of 14.4 Tg CO_2 -C year⁻¹ for the North Slope of Alaska alone is almost identical to an upscaled EC tower flux estimate of 14.27 \pm 3.84 Tg CO_2 -C (Euskirchen et al., 2017). The upscaled EC value was cumulative over two years but was done for subset of tundra vegetation types, which covered half the North Slope area. Both estimates, along with another remote-sensing based upscaling analysis (Ueyama et al., 2013), suggest that tundra is a net CO_2 source to the atmosphere; this finding appears robust across this region using different measurement and scaling techniques.

4.5. Future Site Carbon Dioxide Losses and Constraints

How might these changing conditions and the differential effects on plants and microbes affect C loss from this site in the future? The current rate of loss ($52 \text{ g C m}^{-2} \text{ yr}^{-1}$), if sustained, would lead to $4.18 \text{ kg m}^{-2} \text{ C}$ cumulative loss from 2020 to the end of the century (setting aside other pathways of loss). This amount is 8.4% of the current active layer C pool (49.6 kg C m^{-2} –66 cm depth; Hutchings et al., 2019) projected to be lost as CO_2 by the end of the century. Previous soil radiocarbon work at the site showed that soil surface accumulation may have slowed or even stopped 8–18 years before soil sampling in 2004 (Pries et al., 2012), likely due to conditions that were poor in particular for non-vascular moss growth (Osterkamp et al., 2009). This suggested that the site had shifted from a historical C sink to the observed C source between 1987 and 1997, which independently corresponds to the timing of the documented rapid increase in permafrost temperature at the site. If we make the assumption that the site reached net CO_2 neutrality (annual gains approximately matched annual losses) in 1990, increasing to the observed rate of loss in our time series by 2004, this adds an additional 1.17 kg C m^{-2} cumulative loss between 1990 and 2019 for a total CO_2 loss of 5.33 kg C m^{-2} .

The estimated 8% ecosystem C loss calculation over the next 80 years assumes that future changes in GPP and $R_{\rm eco}$ would remain in lockstep in a warming climate. But the time series suggests that shifting environmental conditions that stimulated plant C uptake and growth were quickly overwhelmed by larger increases in ecosystem C release as a combined result of higher plant and microbial respiration. If future environmental conditions are favourable for microbial activity and $R_{\rm eco}$, the observed net C loss rate averaged for 2014 and 2015 when these conditions occurred in the time series was 130.5 g C m⁻² yr⁻¹, which is 2.5 times the average for the 15-year record. If it took 10 additional years to reach this higher rate (by 2030) with continued environmental change, and which is then sustained to the end of the century, it would

SCHUUR ET AL. 17 of 23



result in a cumulative net CO_2 loss equivalent to $10.00 \text{ kg C m}^{-2}$. If future conditions turn out to be hotter and drier and relatively unfavourable for biological activity, the net C loss rate averaged for 2004 and 2005 when these conditions occurred in the time series was $106.5 \text{ g C m}^{-2} \text{ yr}^{-1}$, which is 2 times the average of our 15-year record. This trajectory would, with the same assumptions as above, result in a cumulative net CO_2 loss of 8.22 kg C m^{-2} . These scenarios represent loss of 20.2% and 16.6% of the current active layer C pool by the end of the century. These also might be minimum estimates because much greater soil C pools would be exposed by continuing permafrost degradation as compared to the size of the thawed soil C pool that influences current observations.

These loss rate calculations based on our 15-year data set are consistent with, and potentially even higher, than earlier calculations from the site (based on 2004–2006 data) that estimated a cumulative net CO_2 loss of 4.4–6.0 kg C m⁻², or 9%–13% of the active layer C, by 2100 (Schuur et al., 2009). Additional measurement years, in particular improved winter C loss estimates, also provided a better estimate of the long-term average NEE. The time series also now includes a wider range of environmental conditions that might be experienced by the site as climate changes in the future. The loss rates calculated in this analysis are similarly consistent with projections from a high latitude laboratory soil C incubation synthesis that estimated potential CO_2 loss between 6%–13% loss for mineral soil horizons (<20% C) and 17%–34% loss for organic soil horizons (>20% C; Schädel et al., 2014); Eight Mile Lake soil profile is a mix of both types of horizons from the surface to 5 m depth.

Factors that might sustain larger C losses relative to C gains in the future include the large soil C pools in permafrost that will thaw with continued warming, and bottlenecks that constrain changes in the plant community more than the microbial community. The time series measurements and the future C loss calculations presented above were limited to the soil C contained in the current active layer. As permafrost degrades, an additional 15 kg C m⁻² will be exposed within the next ~60 cm of soil depth (to 123 cm depth), in addition to the 49.6 kg C m⁻² in the current seasonal active layer (to 66 cm depth; Hutchings et al., 2019; Pries et al., 2012). Beyond that, soil C content at the site initially declines with depth but there is still an additional ~10 kg C m⁻² contained in the next ~150 cm of soil depth (to 3 m depth) and more even deeper. Site projections of future warming will expose at least 3 m of soil (Garnello et al., 2021) and maybe more (SNAP, 2020) to permafrost thaw by 2100, exposing at least an additional 50% more soil C than at present. Community shifts in microbial taxa can happen quickly due to high reproduction rate and short lifespan. These soils already contain large environmental gradients in temperature, moisture, and organic matter quality from surface to depth in the permafrost, and many of the common functions related to soil organic matter decomposition appear to be active in studies of the soil microbial community at the site (Deng et al., 2015; Penton et al., 2016; Xue et al., 2016; Yuan et al., 2018). Taken together, this suggests that our calculations of C loss could reasonably be sustained at the higher end of observed rates in the time series through 2100 and beyond.

In contrast, observed increases in plant C uptake and growth have largely been the result of the response of the extant plant community. Warmer temperatures, a longer growing season, elevated CO2, and most importantly increased nutrient availability from decomposing soil organic matter stimulated plant photosynthesis and growth (Chapin et al., 1995). At the same time, drier conditions caused by a combination of warmer air temperatures and the recession of the water table perched on the permafrost surface acted to limit increases in plant C uptake, with a particular impact on the non-vascular moss and lichen understory (Osterkamp et al., 2009). If future hotter, drier conditions don't reduce plant C uptake from current levels, ecosystem C uptake may persist at levels similar to our measurement record until there is a widespread shift in plant community composition as a result of the colonization of tall shrubs and/or trees with higher C uptake and larger biomass (Chapin et al., 1986; Pugh et al., 2018). Both of these growth forms occur within the nearby area thus seed dispersal is not likely a bottleneck, but the establishment of seedlings on the thick organic layer may instead be a limiting factor to succession (Johnstone, Hollingsworth, et al., 2010). In sum, the slow growth and long lifespan of perennial tundra species, in combination with bottlenecks to plant community change, may continue to limit any further increases in ecosystem C uptake and plant biomass for many decades at this site, with the wildcard of fire that could abruptly change the trajectory (Mack et al., 2011; Young et al., 2017).

SCHUUR ET AL. 18 of 23



Acknowledgments

Funding was provided by a number

of sources: Core funding is current-

ly provided by the NSF Navigating

Additional funding provided by the

Research, Terrestrial Ecosystem Science

(TES) Program Award #DE-SC0006982,

#DE-SC0014085, #DE-SC0020227; Na-

tional Parks Inventory and Monitoring

Program; NSF Bonanza Creek LTER

Program Award #1026415.

U.S. Department of Energy, Office

of Biological and Environmental

the New Arctic Award #1754839.

5. Conclusion

The direct and indirect effects of the changing environment and degrading permafrost have shifted this tundra ecosystem from a historical C sink into a modern C source. The shift is likely to have occurred in the early 1990s in concert with rapid increases in permafrost temperature that were observed at the site, in parallel with other sites across Alaska. While some of the shifting environmental conditions stimulated plant C uptake and growth, these were quickly overwhelmed by larger increases in ecosystem C release as a combined result of higher plant and microbial respiration. If warming conditions continue to promote drying, future increases in plant C uptake may be more limited than increases in ecosystem C release, in part also related to slower successional dynamics of long-lived tundra and boreal plant species. The long-term C exchange time series underscores that widespread warming and thaw across the circumpolar permafrost region has the potential for globally significant net C emissions that would serve to accelerate the rate of climate change, similar in magnitude to other biospheric fluxes such as land use change.

Data Availability Statement

All data are archived in the Bonanza Creek LTER Data Catalog (https://www.lter.uaf.edu) and at Ameriflux (https://ameriflux.lbl.gov).

References

Aubinet, M., Grelle, A., Ibrom, A., Rannik, U., Moncrieff, J., Foken, T., et al. (2000). Estimates of the annual net carbon and water exchange of forests: The EUROFLUX methodology. *Advances in Ecological Research*, 30(30), 113–175.

Baldocchi, D. D. (2003). Assessing the eddy covariance technique for evaluating carbon dioxide exchange rates of ecosystems: Past, present and future. Global Change Biology, 9(4), 479–492. https://doi.org/10.1046/j.1365-2486.2003.00629.x

Beck, P. S. A., Juday, G. P., Alix, C., Barber, V. A., Winslow, S. E., Sousa, E. E., et al. (2011). Changes in forest productivity across Alaska consistent with biome shift. *Ecology Letters*, 14(4), 373–379. https://doi.org/10.1111/j.1461-0248.2011.01598.x

Belshe, E. F., Schuur, E. A. G., & Bolker, B. M. (2013). Tundra ecosystems observed to be CO_2 sources due to differential amplification of the carbon cycle. *Ecology Letters*, 16(10), 1307–1315. https://doi.org/10.1111/ele.12164

Belshe, E. F., Schuur, E. A. G., Bolker, B. M., & Bracho, R. (2012). Incorporating spatial heterogeneity created by permafrost thaw into a landscape carbon estimate. *Journal of Geophysical Research*, 117, G01026. https://doi.org/10.1029/2011jg001836

Bhatt, U. S., Walker, D. A., Raynolds, M. K., Bieniek, P. A., Epstein, H. E., Comiso, J. C., et al. (2017). Changing seasonality of panarctic tundra vegetation in relationship to climatic variables. *Environmental Research Letters*, 12(5). https://doi.org/10.1088/1748-9326/aa6b0b Bieniek, P. A., Bhatt, U. S., Thoman, R. L., Angeloff, H., Partain, J., Papineau, J., et al. (2012). Climate divisions for Alaska based on objective methods. *Journal of Applied Meteorology and Climatology*, 51(7), 1276–1289. https://doi.org/10.1175/jamc-d-11-0168.1

Biskaborn, B. K., Smith, S. L., Noetzli, J., Matthes, H., Vieira, G., Streletskiy, D. A., et al. (2019). Permafrost is warming at a global scale. *Nature Communications*, 10. https://doi.org/10.1038/s41467-018-08240-4

Bjerke, J. W., Treharne, R., Vikhamar-Schuler, D., Karlsen, S. R., Ravolainen, V., Bokhorst, S., et al. (2017). Understanding the drivers of extensive plant damage in boreal and Arctic ecosystems: Insights from field surveys in the aftermath of damage. *Science of the Total Environment*, 599–600, 1965–1976. https://doi.org/10.1016/j.scitotenv.2017.05.050

Boelman, N. T., Stieglitz, M., Rueth, H. M., Sommerkorn, M., Griffin, K. L., Shaver, G. R., & Gamon, J. A. (2003). Response of NDVI, biomass, and ecosystem gas exchange to long-term warming and fertilization in wet sedge tundra. *Oecologia*, 135(3), 414–421. https://doi.org/10.1007/s00442-003-1198-3

Bracho, R., Natali, S., Pegoraro, E., Crummer, K. G., Schädel, C., Celis, G., et al. (2016). Temperature sensitivity of organic matter decomposition of permafrost-region soils during laboratory incubations. *Soil Biology and Biochemistry*, 97, 1–14. https://doi.org/10.1016/j. soilbio.2016.02.008

Brown, J., Ferrians, J. O., Heginbottom, J. A., & Melnikov, E. S. (1998). Circum-Arctic map of permafrost and ground-ice conditions. National Snow and Ice Data Center/World Data Center for Glaciology.

Brown, J., & Romanovsky, V. E. (2008). Report from the international permafrost association: State of permafrost in the first decade of the 21st century. *Permafrost and Periglacial Processes*, 19(2), 255–260. https://doi.org/10.1002/ppp.618

Burba, G. G., McDermitt, D. K., Grelle, A., Anderson, D. J., & Xu, L. (2008). Addressing the influence of instrument surface heat exchange on the measurements of CO₂ flux from open-path gas analyzers. *Global Change Biology*, 14(8), 1854–1876. https://doi.org/10.1111/j.1365-2486.2008.01606.x

Celis, G., Mauritz, M., Bracho, R., Salmon, V. G., Webb, E. E., Hutchings, J., et al. (2017). Tundra is a consistent source of CO₂ at a site with progressive permafrost thaw during 6 years of chamber and eddy covariance measurements. *Journal of Geophysical Research: Biogeosciences*, 122(6), 1471–1485. https://doi.org/10.1002/2016jg003671

Chapin, F. S., Shaver, G. R., Giblin, A. E., Nadelhoffer, K. J., & Laundre, J. A. (1995). Responses of arctic tundra to experimental and observed changes in climate. *Ecology*, 76(3), 694–711. https://doi.org/10.2307/1939337

Chapin, F. S., Vitousek, P. M., & Van Cleve, K. (1986). The nature of nutrient limitation in plant communities. *The American Naturalist*, 127(1), 48–58. https://doi.org/10.1086/284466

Chapin, F. S., Woodwell, G. M., Randerson, J. T., Rastetter, E. B., Lovett, G. M., Baldocchi, D. D., et al. (2006). Reconciling carbon-cycle concepts, terminology, and methods. *Ecosystems*, 9(7), 1041–1050. https://doi.org/10.1007/s10021-005-0105-7

Chen, J., Jonsson, P., Tamura, M., Gu, Z. H., Matsushita, B., & Eklundh, L. (2004). A simple method for reconstructing a high-quality NDVI time-series data set based on the Savitzky-Golay filter. *Remote Sensing of Environment*, 91(3-4), 332-344. https://doi.org/10.1016/j.rse.2004.03.014

SCHUUR ET AL. 19 of 23



- Commane, R., Lindaas, J., Benmergui, J., Luus, K. A., Chang, R. Y.-W., Daube, B. C., et al. (2017). Carbon dioxide sources from Alaska driven by increasing early winter respiration from Arctic tundra. Proceedings of the National Academy of Sciences of the United States of America, 114(21), 5361–5366. https://doi.org/10.1073/pnas.1618567114
- Davidson, E. A., & Janssens, I. A. (2006). Temperature sensitivity of soil carbon decomposition and feedbacks to climate change. *Nature*, 440(7081), 165–173. https://doi.org/10.1038/nature04514
- Deane-Coe, K. K., Mauritz, M., Celis, G., Salmon, V., Crummer, K. G., Natali, S. M., & Schuur, E. A. G. (2015). Experimental warming alters productivity and isotopic signatures of tundra mosses. *Ecosystems*, 18(6), 1070–1082. https://doi.org/10.1007/s10021-015-9884-7
- Deng, J., Gu, Y., Zhang, J., Xue, K., Qin, Y., Yuan, M., et al. (2015). Shifts of tundra bacterial and archaeal communities along a permafrost thaw gradient in Alaska. *Molecular Ecology*, 24(1), 222–234. https://doi.org/10.1111/mec.13015
- Didan, K., Munoz, A. B., Solano, R., & Huete, A. R. (2015). MODIS, vegetation index user's guide the univesity of Arizona, (p. 32).
- DOE. (2020). U.S. Department of Energy free-air CO² enrichment experiments: FACE results, lessons, and legacy. U.S. Department of Energy. Euskirchen, E. S., Bret-Harte, M. S., Shaver, G. R., Edgar, C. W., & Romanovsky, V. E. (2017). Long-term release of carbon dioxide from Arctic tundra ecosystems in Alaska. Ecosystems, 20(5), 960–974. https://doi.org/10.1007/s10021-016-0085-9
- Euskirchen, E. S., Edgar, C. W., Turetsky, M. R., Waldrop, M. P., & Harden, J. W. (2014). Differential response of carbon fluxes to climate in three peatland ecosystems that vary in the presence and stability of permafrost. *Journal of Geophysical Research: Biogeosciences*, 119(8), 1576–1595. https://doi.org/10.1002/2014jg002683
- Euskirchen, E. S., McGuire, A. D., Kicklighter, D. W., Zhuang, Q., Clein, J. S., Dargaville, R. J., et al. (2006). Importance of recent shifts in soil thermal dynamics on growing season length, productivity, and carbon sequestration in terrestrial high-latitude ecosystems. *Global Change Biology*, 12(4), 731–750. https://doi.org/10.1111/j.1365-2486.2006.01113.x
- Falge, E., Baldocchi, D., Olson, R., Anthoni, P., Aubinet, M., Bernhofer, C., et al. (2001). Gap filling strategies for defensible annual sums of net ecosystem exchange. Agricultural and Forest Meteorology, 107(1), 43–69. https://doi.org/10.1016/s0168-1923(00)00225-2
- Foken, T., Gockede, M., Mauder, M., Mahrt, L., Amiro, B., & Munger, W. (2004). Post-field data quality control. In X. Lee, W. Massman, & B. Law (Eds.), *Handbook of micrometeorology* (pp. 181–208). Kluwer Academic Publishers.
- Foken, T., Meixner, F. X., Falge, E., Zetzsch, C., Serafimovich, A., Bargsten, A., et al. (2012). Coupling processes and exchange of energy and reactive and non-reactive trace gases at a forest site–results of the EGER experiment. *Atmospheric Chemistry and Physics*, 12(4), 1923–1950. https://doi.org/10.5194/acp-12-1923-2012
- Friebel, H. C., Herrington, T. O., & Benilov, A. Y. (2009). Evaluation of the flow distortion around the campbell scientific CSAT3 sonic anemometer relative to incident wind direction. *Journal of Atmospheric and Oceanic Technology*, 26(3), 582–592. https://doi.org/10.1175/2008jtecho550.1
- Garnello, A. J., Celis, G., Ledman, J., Luo, Y., Nicolsky, D., Romanovsky, V., & Schuur, E. A. G. (2021). Forecasting permafrost thaw of sub-Arctic tundra with a thermodynamic model calibrated to site measurements. *Journal of Geophysical Research: Biogeosciences*. Submitted.
- Grant, R. F., Humphreys, E. R., Lafleur, P. M., & Dimitrov, D. D. (2011). Ecological controls on net ecosystem productivity of a mesic arctic tundra under current and future climates. *Journal of Geophysical Research*, 116. https://doi.org/10.1029/2010jg001555
- Gruber, S. (2012). Derivation and analysis of a high-resolution estimate of global permafrost zonation. *The Cryosphere*, 6(1), 221–233. https://doi.org/10.5194/tc-6-221-2012
- Hall, D. K., & Riggs, G. A. (2016). MODIS/Aqua snow cover daily L3 global 500m SIN grid. Version 6. NASA national snow and ice data. Center Distributed Active Center.
- Harden, J. W., Mark, R. K., Sundquist, E. T., & Stallard, R. F. (1992). Dynamics of soil carbon during deglaciation of the Laurentide ice sheet. Science, 258(5090), 1921–1924. https://doi.org/10.1126/science.258.5090.1921
- Hewitt, R. E., Taylor, D. L., Genet, H., McGuire, A. D., & Mack, M. C. (2019). Below-ground plant traits influence tundra plant acquisition of newly thawed permafrost nitrogen. *Journal of Ecology*, 107(2), 950–962. https://doi.org/10.1111/1365-2745.13062
- Hollinger, D. Y., & Richardson, A. D. (2005). Uncertainty in eddy covariance measurements and its application to physiological models. *Tree Physiology*, 25(7), 873–885. https://doi.org/10.1093/treephys/25.7.873
- Hothorn, T., Hornik, K., & Zeileis, A. (2006). Unbiased recursive partitioning: A conditional inference framework. *Journal of Computational and Graphical Statistics*, 15(3), 651–674. https://doi.org/10.1198/106186006x133933
- Hothorn, T., & Zeileis, A. (2015). Partykit: A modular toolkit for recursive partytioning in R. Journal of Machine Learning Research, 16, 3905–3909.
- Hugelius, G., Strauss, J., Zubrzycki, S., Harden, J. W., Schuur, E. A. G., Ping, C.-L., et al. (2014). Estimated stocks of circumpolar permafrost carbon with quantified uncertainty ranges and identified data gaps. *Biogeosciences*, 11(23), 6573–6593. https://doi.org/10.5194/bg-11-6573-2014
- Hutchings, J. A., Bianchi, T. S., Kaufman, D. S., Kholodov, A. L., Vaughn, D. R., & Schuur, E. A. G. (2019). Millennial-scale carbon accumulation and molecular transformation in a permafrost core from Interior Alaska. Geochimica Et Cosmochimica Acta, 253, 231–248. https://doi.org/10.1016/j.gca.2019.03.028
- IPCC. (2013). Climate change 2013: The physical science basis. In Contribution of working group I to the fifth assessment report of the intergovernmental panel on climate change. Cambridge University Press.
- IPCC. (2018). Global Warming of 1.5°C. In An IPCC Special Report on the impacts of global warming of 1.5°C above pre-industrial levels and related global greenhouse gas emission pathways, in the context of strengthening the global response to the threat of climate change, sustainable development, and efforts to eradicate poverty.
- Jiang, M., Medlyn, B. E., Drake, J. E., Duursma, R. A., Anderson, I. C., Barton, C. V. M., et al. (2020). The fate of carbon in a mature forest under carbon dioxide enrichment. *Nature*, 580(7802), 227–231. https://doi.org/10.1038/s41586-020-2128-9
- Jobbágy, E. G., & Jackson, R. B. (2000). The vertical distribution of soil organic carbon and its relation to climate and vegetation. *Ecological Applications*, 10(2), 423–436. https://doi.org/10.1890/1051-0761(2000)010[0423:tvdoso]2.0.co;2
- Johnstone, J. F., Chapin, F. S., Hollingsworth, T. N., Mack, M. C., Romanovsky, V., & Turetsky, M. (2010). Fire, climate change, and forest resilience in interior Alaska this article is one of a selection of papers from the dynamics of change in Alaska's Boreal Forests: Resilience and vulnerability in response to climate warming. Canadian Journal of Forest Research, 40(7), 1302–1312. https://doi.org/10.1139/ x10-061
- Johnstone, J. F., Hollingsworth, T. N., Chapin, F. S., & Mack, M. C. (2010). Changes in fire regime break the legacy lock on successional trajectories in Alaskan boreal forest. *Global Change Biology*, 16(4), 1281–1295. https://doi.org/10.1111/j.1365-2486.2009.02051.x
- Ju, J., & Masek, J. G. (2016). The vegetation greenness trend in Canada and US Alaska from 1984-2012 Landsat data. Remote Sensing of Environment, 176, 1–16. https://doi.org/10.1016/j.rse.2016.01.001

SCHUUR ET AL. 20 of 23



- Keuper, F., Parmentier, F.-J. W., Blok, D., van Bodegom, P. M., Dorrepaal, E., van Hal, J. R., et al. (2012). Tundra in the rain: Differential vegetation responses to three years of experimentally doubled summer precipitation in Siberian shrub and Swedish bog tundra. *Ambio*, 41, 269–280. https://doi.org/10.1007/s13280-012-0305-2
- Kirschbaum, M. U. F. (2000). Will changes in soil organic carbon act as a positive or negative feedback on global warming? *Biogeochemistry*, 48(1), 21–51. https://doi.org/10.1023/a:1006238902976
- Kormann, R., & Meixner, F. X. (2001). An analytical footprint model for non-neutral stratification. Boundary-Layer Meteorology, 99(2), 207–224. https://doi.org/10.1023/a:1018991015119
- Koven, C. D., Riley, W. J., & Stern, A. (2013). Analysis of permafrost thermal dynamics and response to climate change in the CMIP5 Earth system models. *Journal of Climate*, 26(6), 1877–1900. https://doi.org/10.1175/jcli-d-12-00228.1
- Koven, C. D., Schuur, E. A. G., Schädel, C., Bohn, T. J., Burke, E. J., Chen, G., et al. (2015). A simplified, data-constrained approach to estimate the permafrost carbon-climate feedback. *Philosophical Transactions of the Royal Society A-Mathematical Physical and Engineering Sciences*, 373(2054), https://doi.org/10.1098/rsta.2014.0423
- Lara, M. J., Nitze, I., Grosse, G., & McGuire, A. D. (2018). Tundra landform and vegetation productivity trend maps for the Arctic Coastal Plain of northern Alaska. *Scientific Data*, 5. https://doi.org/10.1038/sdata.2018.58
- Liu, M., He, H., Yu, G., Luo, Y., Sun, X., & Wang, H. (2009). Uncertainty analysis of CO₂ flux components in subtropical evergreen coniferous plantation. Science in China–Series D: Earth Sciences, 52(2), 257–268. https://doi.org/10.1007/s11430-009-0010-6
- Lund, M., Lafleur, P. M., Roulet, N. T., Lindroth, A., Christensen, T. R., Aurela, M., et al. (2010). Variability in exchange of CO₂ across 12 northern peatland and tundra sites. *Global Change Biology*, 16(9), 2436–2448.
- Mack, M. C., Bret-Harte, M. S., Hollingsworth, T. N., Jandt, R. R., Schuur, E. A. G., Shaver, G. R., & Verbyla, D. L. (2011). Carbon loss from an unprecedented Arctic tundra wildfire. *Nature*, 475(7357), 489–492. https://doi.org/10.1038/nature10283
- Mauritz, M., Bracho, R., Celis, G., Hutchings, J., Natali, S. M., Pegoraro, E., et al. (2017). Nonlinear CO₂ flux response to 7 years of experimentally induced permafrost thaw. Global Change Biology, 23(9), 3646–3666. https://doi.org/10.1111/gcb.13661
- McGuire, A. D., Christensen, T. R., Hayes, D., Heroult, A., Euskirchen, E., Kimball, J. S., et al. (2012). An assessment of the carbon balance of Arctic tundra: Comparisons among observations, process models, and atmospheric inversions. *Biogeosciences*, 9(8), 3185–3204. https://doi.org/10.5194/bg-9-3185-2012
- McGuire, A. D., Koven, C., Lawrence, D. M., Clein, J. S., Xia, J., Beer, C., et al. (2016). Variability in the sensitivity among model simulations of permafrost and carbon dynamics in the permafrost region between 1960 and 2009. *Global Biogeochemical Cycles*, 30(7), 1015–1037. https://doi.org/10.1002/2016gb005405
- McGuire, A. D., Lawrence, D. M., Koven, C., Clein, J. S., Burke, E., Chen, G., et al. (2018). Dependence of the evolution of carbon dynamics in the northern permafrost region on the trajectory of climate change. *Proceedings of the National Academy of Sciences of the United States of America*, 115(15), 3882–3887. https://doi.org/10.1073/pnas.1719903115
- Meredith, M., Sommerkorn, M., Cassotta, S., Derksen, C., Ekaykin, A., Hollowed, A., et al. (2019). Polar Regions. In H.-O. Pörtner, D. C. Roberts, V. Masson-Delmotte, P. Zhai, M. Tignor, E. Poloczanska, et al. (Eds.), *IPCC special report on the ocean and cryosphere in a changing climate*.
- Mueller, C. W., Rethemeyer, J., Kao-Kniffin, J., Löppmann, S., Hinkel, K. M., & G. Bockheim, J. (2015). Large amounts of labile organic carbon in permafrost soils of northern Alaska. *Global Change Biology*, 21(7), 2804–2817. https://doi.org/10.1111/gcb.12876
- Natali, S. M., Schuur, E. A. G., Mauritz, M., Schade, J. D., Celis, G., Crummer, K. G., et al. (2015). Permafrost thaw and soil moisture driving CO₂ and CH₄ release from upland tundra. *Journal of Geophysical Research: Biogeosciences.*, 120(3), 525–537. https://doi.org/10.1002/2014jg002872
- Natali, S. M., Schuur, E. A. G., & Rubin, R. L. (2012). Increased plant productivity in Alaskan tundra as a result of experimental warming of soil and permafrost. *Journal of Ecology*, 100(2), 488–498. https://doi.org/10.1111/j.1365-2745.2011.01925.x
- Natali, S. M., Watts, J. D., Rogers, B. M., Potter, S., Ludwig, S. M., Selbmann, A.-K., et al. (2019). Large loss of CO² in winter observed across the northern permafrost region. *Nature Climate Change*, 9(11), 852–857. https://doi.org/10.1038/s41558-019-0592-8
- NOAA. (2019). National centers for environmental information, climate at a glance: Divisional time series. NOAA.
- Obu, J., Westermann, S., Bartsch, A., Berdnikov, N., Christiansen, H. H., Dashtseren, A., et al. (2019). Northern hemisphere permafrost map based on TTOP modelling for 2000-2016 at 1 km² scale. *Earth-Science Reviews*, 193, 299–316. https://doi.org/10.1016/j.earscirev.2019.04.023
- Oechel, W. C., Laskowski, C. A., Burba, G., Gioli, B., & Kalhori, A. A. M. (2014). Annual patterns and budget of CO₂ flux in an Arctic tussock tundra ecosystem. *Journal of Geophysical Research: Biogeosciences*, 119(3), 323–339. https://doi.org/10.1002/2013jg002431
- Osterkamp, T. E., Jorgenson, M. T., Schuur, E. A. G., Shur, Y. L., Kanevskiy, M. Z., Vogel, J. G., & Tumskoy, V. E. (2009). Physical and ecological changes associated with warming permafrost and thermokarst in interior Alaska. *Permafrost and Periglacial Processes*, 20(3), 235–256. https://doi.org/10.1002/ppp.656
- Osterkamp, T. E., & Romanovsky, V. E. (1999). Evidence for warming and thawing of discontinuous permafrost in Alaska. *Permafrost and Periglacial Processes*, 10(1), 17–37. https://doi.org/10.1002/(sici)1099-1530(199901/03)10:1<17::aid-ppp303>3.0.co;2-4
- Overland, J. E., Wang, M., Walsh, J. E., & Stroeve, J. C. (2014). Future Arctic climate changes: Adaptation and mitigation time scales. *Earth's Future*, 2(2), 68–74. https://doi.org/10.1002/2013ef000162
- Overland, J., Walsh, J., & Kattsov, V. (2017). Trends and feedbacks, Arctic monitoring and assessment Program.
- Parmentier, F. J. W., van der Molen, M. K., van Huissteden, J., Karsanaev, S. A., Kononov, A. V., Suzdalov, D. A., et al. (2011). Longer growing seasons do not increase net carbon uptake in the northeastern Siberian tundra. *Journal of Geophysical Research*, 116. https://doi.org/10.1029/2011jg001653
- Penton, C. R., Yang, C. Y., Wu, L. Y., Wang, Q., Zhang, J., Liu, F. F., et al. (2016). NifH-harboring bacterial community composition across an Alaskan permafrost thaw gradient. Frontirs in Microbiology, 7. https://doi.org/10.3389/fmicb.2016.01894
- Phoenix, G. K., & Bjerke, J. W. (2016). Arctic browning: Extreme events and trends reversing arctic greening. *Global Change Biology*, 22(9), 2960–2962. https://doi.org/10.1111/gcb.13261
- Pithan, F., & Mauritsen, T. (2014). Arctic amplification dominated by temperature feedbacks in contemporary climate models. *Nature Geoscience*, 7(3), 181–184. https://doi.org/10.1038/ngeo2071
- Pries, C. E. H., Schuur, E. A. G., & Crummer, K. G. (2012). Holocene carbon stocks and carbon accumulation rates altered in soils undergoing permafrost thaw. *Ecosystems*, 15(1), 162–173.
- Pries, C. E. H., Schuur, E. A. G., Vogel, J. G., & Natali, S. M. (2013). Moisture drives surface decomposition in thawing tundra. *Journal of Geophysical Research: Biogeosciences*, 118(3), 1133–1143. https://doi.org/10.1002/jgrg.20089
- Pugh, T. A. M., Jones, C. D., Huntingford, C., Burton, C., Arneth, A., Brovkin, V., et al. (2018). A large committed long-term sink of carbon due to vegetation dynamics. *Earth's Future*, 6(10), 1413–1432. https://doi.org/10.1029/2018ef000935

SCHUUR ET AL. 21 of 23



- Raz-Yaseef, N., Torn, M. S., Wu, Y., Billesbach, D. P., Liljedahl, A. K., Kneafsey, T. J., et al. (2017). Large CO₂ and CH₄ emissions from polygonal tundra during spring thaw in northern Alaska. *Geophysical Research Letters*, 44(1), 504–513. https://doi.org/10.1002/2016gl071220 R Core Team (2018). R: A Language and Environment for Statistical Computing. Vienna: R Foundation for Statistical Computing. https://
- www.R-project.org
 Riahi, K., Rao, S., Krey, V., Cho, C. H., Chirkov, V., Fischer, G., et al. (2011). RCP 8.5-A scenario of comparatively high greenhouse gas emissions. Climatic Change, 109(1–2), 33–57. https://doi.org/10.1007/s10584-011-0149-y
- Romanovsky, V. E., Smith, S. L., Christiansen, H. H., Shiklomanov, N. I., Streletskiy, D. A., Drozdov, D. S., et al. (2012). Permafrost in Arctic Report Card 2012. NOAA.
- Romanovsky, V., Isaksen, K., Drozdov, D., Anisimov, O., Instanes, A., Leibman, M., et al. (2017). Changing permafrost and its impact, arctic monitoring and assessment programme (AMAP).
- Rustad, L., Campbell, J. L., Campbell, J., Marion, G., Norby, R., Mitchell, M., et al. (2001). A meta-analysis of the response of soil respiration, net nitrogen mineralization, and aboveground plant growth to experimental ecosystem warming. *Oecologia*, 126(4), 543–562. https://doi.org/10.1007/s004420000544
- Salmon, V. G., Soucy, P., Mauritz, M., Celis, G., Natali, S. M., Mack, M. C., & Schuur, E. A. G. (2016). Nitrogen availability increases in a tundra ecosystem during five years of experimental permafrost thaw. *Global Change Biology*, 22(5), 1927–1941. https://doi.org/10.1111/gch.13204
- Schädel, C., Bader, M. K.-F., Schuur, E. A. G., Biasi, C., Bracho, R., Čapek, P., et al., 2016. Potential carbon emissions dominated by carbon dioxide from thawed permafrost soils. *Nature Climate Change*, 6(10): 950-+. https://doi.org/10.1038/nclimate3054
- Schädel, C., Schuur, E. A. G., Bracho, R., Elberling, B., Knoblauch, C., Lee, H., et al. (2014). Circumpolar assessment of permafrost C quality and its vulnerability over time using long-term incubation data. *Global Change Biology*, 20(2), 641–652.
- Schotanus, P., Nieuwstadt, F. T. M., & De Bruin, H. A. R. (1983). Temperature measurement with a sonic anemometer and its application to heat and moisture fluxes. $Boundary-Layer\ Meteorology, 26(1), 81-93.\ https://doi.org/10.1007/bf00164332$
- Schuur, E. A. G., & Abbott, B. (2011). High risk of permafrost thaw. Nature, 480(7375), 32–33. https://doi.org/10.1038/480032a
- Schuur, E. A. G., Abbott, B. W., Bowden, W. B., Brovkin, V., Camill, P., Canadell, J. G., et al. (2013). Expert assessment of vulnerability of permafrost carbon to climate change. Climatic Change, 119(2), 359–374. https://doi.org/10.1007/s10584-013-0730-7
- Schuur, E. A. G., Bockheim, J., Canadell, J. G., Euskirchen, E., Field, C. B., Goryachkin, S. V., et al. (2008). Vulnerability of permafrost carbon to climate change: Implications for the global carbon cycle. *Bioscience*, 58(8), 701–714. https://doi.org/10.1641/b580807
- Schuur, E. A. G., Crummer, K. G., Vogel, J. G., & Mack, M. C. (2007). Plant species composition and productivity following permafrost thaw and thermokarst in Alaskan tundra. *Ecosystems*, 10(2), 280–292. https://doi.org/10.1007/s10021-007-9024-0
- Schuur, E. A. G., & Mack, M. C. (2018). Ecological response to permafrost thaw and consequences for local and global ecosystem services. In D. J. Futuyma (Ed.), Annual review of ecology, evolution, and systematics (49, pp. 279–301).
- Schuur, E. A. G., McGuire, A. D., Romanovsky, V., Schädel, C., & Mack, M. C. (2018). Arctic and boreal carbon. U.S. Global Change Research Program
- Schuur, E. A. G., McGuire, A. D., Schädel, C., Grosse, G., Harden, J. W., Hayes, D. J., et al. (2015). Climate change and the permafrost carbon feedback. *Nature*, 520(7546), 171–179. https://doi.org/10.1038/nature14338
- Schuur, E. A. G., Vogel, J. G., Crummer, K. G., Lee, H., Sickman, J. O., & Osterkamp, T. E. (2009). The effect of permafrost thaw on old carbon release and net carbon exchange from tundra. *Nature*, 459, 556–559. https://doi.org/10.1038/nature08031
- Shaver, G. R., Canadell, J., Chapin, F. S., Gurevitch, J., Harte, J., Henry, G., et al. (2000). Global warming and terrestrial ecosystems: A conceptual framework for analysis. *Bioscience*, 50(10), 871–882. https://doi.org/10.1641/0006-3568(2000)050[0871:gwatea]2.0.co;2
- Shaver, G. R., Giblin, A. E., Nadelhoffer, K. J., Thieler, K. K., Downs, M. R., Laundre, J. A., & Rastetter, E. B. (2006). Carbon turnover in Alaskan tundra soils: Effects of organic matter quality, temperature, moisture and fertilizer. *Journal of Ecology*, 94(4), 740–753. https://doi.org/10.1111/j.1365-2745.2006.01139.x
- SNAP. (2020). GIPL model outputs-linear coupled-annual scenarios network for Alaska and Arctic planning. In *U.o.A. International Arctic Research Center*. Fairbanks.
- Soil Survey Staff. (2014). Keys to soil taxonomy. USDA-Natural Resources Conservation Service.
- Strauss, J., Schirrmeister, L., Grosse, G., Fortier, D., Hugelius, G., Knoblauch, C., et al. (2017). Deep yedoma permafrost: A synthesis of depositional characteristics and carbon vulnerability. Earth-Science Reviews, 172, 75–86. https://doi.org/10.1016/j.earscirev.2017.07.007
- Taylor, M. A., Celis, G., Ledman, J. D., Bracho, R., & Schuur, E. A. G. (2018). Methane efflux measured by eddy covariance in Alaskan upland tundra undergoing permafrost degradation. *Journal of Geophysical Research: Biogeosciences.*, 123(9), 2695–2710. https://doi. org/10.1029/2018jg004444
- Trucco, C., Schuur, E. A. G., Natali, S. M., Belshe, E. F., Bracho, R., & Vogel, J. (2012). Seven-year trends of CO₂ exchange in a tundra ecosystem affected by long-term permafrost thaw. *Journal of Geophysical Research*, 117. https://doi.org/10.1029/2011jg001907
- Ueyama, M., Ichii, K., Iwata, H., Euskirchen, E. S., Zona, D., Rocha, A. V., et al. (2013). Upscaling terrestrial carbon dioxide fluxes in Alaska with satellite remote sensing and support vector regression. *Journal of Geophysical Research: Biogeosciences*, 118(3), 1266–1281. https://doi.org/10.1002/jgrg.20095
- Vogel, J., Schuur, E. A. G., Trucco, C., & Lee, H. (2009). Response of CO₂ exchange in a tussock tundra ecosystem to permafrost thaw and thermokarst development. *Journal of Geophysical Research*, 114(G4), G04018. https://doi.org/10.1029/2008jg000901
- Walsh, J. E., Bieniek, P. A., Brettschneider, B., Euskirchen, E. S., Lader, R., & Thoman, R. L. (2017). The exceptionally warm winter of 2015/16 in Alaska. *Journal of Climate*, 30(6), 2069–2088. https://doi.org/10.1175/jcli-d-16-0473.1
- Webb, E. E., Schuur, E. A. G., Natali, S. M., Oken, K. L., Bracho, R., Krapek, J. P., et al. (2016). Increased wintertime CO₂ loss as a result of sustained tundra warming. *Journal of Geophysical Research: Biogeosciences*, 121(2), 249–265. https://doi.org/10.1002/2014jg002795
- Webb, E. K., Pearman, G. I., & Leuning, R. (1980). Correction of flux measurements for density effects due to heat and water vapour transfer. Quarterly Journal of the Royal Meteorological Society, 106(447), 85–100. https://doi.org/10.1002/qj.49710644707
- Winton, M. (2006). Amplified Arctic climate change: What does surface albedo feedback have to do with it? *Geophysical Research Letters*, 33(3). https://doi.org/10.1029/2005gl025244
- Xue, K., M. Yuan, M., J. Shi, Z., Qin, Y., Deng, Y., Cheng, L., et al. (2016). Tundra soil carbon is vulnerable to rapid microbial decomposition under climate warming. *Nature Climate Change*, 6(6): 595–600. https://doi.org/10.1038/nclimate2940
- Young, A. M., Higuera, P. E., Duffy, P. A., & Hu, F. S. (2017). Climatic thresholds shape northern high-latitude fire regimes and imply vulnerability to future climate change. *Ecography*, 40(5), 606–617. https://doi.org/10.1111/ecog.02205
- Yuan, M. M., Zhang, J., Xue, K., Wu, L., Deng, Y., Deng, J., et al. (2018). Microbial functional diversity covaries with permafrost thaw-induced environmental heterogeneity in tundra soil. *Global Change Biology*, 24(1), 297–307. https://doi.org/10.1111/gcb.13820

SCHUUR ET AL. 22 of 23



10.1029/2020JG006044



- Yuan, W. P., Zheng, Y., Piao, S. L., Ciais, P., Lombardozzi, D., Wang, Y. P., et al. (2019). Increased atmospheric vapor pressure deficit reduces global vegetation growth. Science Advances, 5(8). https://doi.org/10.1126/sciadv.aax1396
- Zhang, T., Heginbottom, J. A., Barry, R. G., & Brown, J. (2000). Further statistics on the distribution of permafrost and ground ice in the northern hemisphere 1. *Polar Geography*, 24(2), 126–131. https://doi.org/10.1080/10889370009377692
- Zhuang, Q. L., Melillo, J. M., Sarofim, M. C., Kicklighter, D. W., McGuire, A. D., Felzer, B. S., et al. (2006). CO_2 and CH_4 exchanges between land ecosystems and the atmosphere in northern high latitudes over the 21st century. *Geophysical Research Letters*, 33(17). https://doi.org/10.1029/2006gl026972
- Zimov, S. A., Schuur, E. A. G., & Chapin, F. S. (2006). Climate change: Permafrost and the global carbon budget. *Science*, 312(5780), 1612–1613. https://doi.org/10.1126/science.1128908

SCHUUR ET AL. 23 of 23